ASTROBIOLOGY
Volume 5, Number 3, 2005

Research Paper

Raman Imagery: A New Approach to Assess the Geochemical Maturity and Biogenicity of Permineralized Precambrian Fossils

J. WILLIAM SCHOPF,[1–4] ANATOLIY B. KUDRYAVTSEV,[2,4] DAVID G. AGRESTI,[5] ANDREW D. CZAJA,[1,2] and THOMAS J. WDOWIAK[5]

ABSTRACT

Laser-Raman imagery is a non-intrusive, non-destructive analytical technique, recently introduced to Precambrian paleobiology, that can be used to demonstrate a one-to-one spatial correlation between the optically discernible morphology and kerogenous composition of permineralized fossil microorganisms. Made possible by the submicron-scale resolution of the technique and its high sensitivity to the Raman signal of carbonaceous matter, such analyses can be used to determine the chemical–structural characteristics of organic-walled microfossils and associated sapropelic carbonaceous matter in acid-resistant residues and petrographic thin sections. Here we use this technique to analyze kerogenous microscopic fossils and associated carbonaceous sapropel permineralized in 22 unmetamorphosed or little-metamorphosed fine-grained chert units ranging from ~400 to ~2,100 Ma old. The lineshapes of the Raman spectra acquired vary systematically with five indices of organic geochemical maturation: (1) the mineral-based metamorphic grade of the fossil-bearing units; (2) the fidelity of preservation of the fossils studied; (3) the color of the organic matter analyzed; and both the (4) H/C and (5) N/C ratios measured in particulate kerogens isolated from bulk samples of the fossil-bearing cherts. Deconvolution of relevant spectra shows that those of relatively well-preserved permineralized kerogens analyzed *in situ* exhibit a distinctive set of Raman bands that are identifiable also in hydrated organic-walled microfossils and particulate carbonaceous matter freed from the cherts by acid maceration. These distinctive Raman bands, however, become indeterminate upon dehydration of such specimens. To compare quantitatively the variations observed among the spectra measured, we introduce the Raman Index of Preservation, an approximate measure of the geochemical maturity of the kerogens studied that is consistent both with the five indices of organic geochemical alteration and with spectra acquired from fossils experimentally heated under controlled laboratory conditions.

[1]Department of Earth & Space Sciences, [2]Institute of Geophysics & Planetary Physics (Center for the Study of Evolution and the Origin of Life), [3]Molecular Biology Institute, and [4]NASA Astrobiology Institute, University of California, Los Angeles, California.

[5]Astro & Solar System Physics Program, Department of Physics, and Center for Biophysical Sciences and Engineering, University of Alabama at Birmingham, Birmingham, Alabama.

The results reported provide new insight into the chemical–structural characteristics of ancient carbonaceous matter, the physicochemical changes that accompany organic geochemical maturation, and a new criterion to be added to the suite of evidence by which to evaluate the origin of minute fossil-like objects of possible but uncertain biogenicity. Key Words: Raman spectroscopic imagery—Raman Index of Preservation—Precambrian fossils—Kerogen maturation—Biogenicity. Astrobiology 5, 333–371.

INTRODUCTION

As the field of astrobiology has come to the fore, it has become increasingly recognized that the search for life elsewhere in the Cosmos should be centered on a search for evidence of microbe-level living systems—whether ancient or extant. In part, this strategy rests on the seemingly well-grounded assumption that "simple" forms of life, such as microbes, can be expected to exist whether or not more advanced organisms have subsequently arisen. Chiefly, however, it is based on the realization that throughout biologic history microbe-level life has been ubiquitous, abundant, metabolically diverse, and [for the earliest (Precambrian) seven-eighths of geological time] biotically predominant. In the search for life elsewhere, the microbe-dominated world of the Precambrian is the best analogue we know.

Lessons learned from studies of the Precambrian fossil record may thus be key to the search for evidence of ancient life on other worlds. Perhaps foremost among such lessons is an awareness of the difficulty inherent in establishing the biogenicity of minute fossil-like objects, the challenging problem of unambiguously distinguishing true biologic remnants from non-biologic look-alikes (*cf*. Cady *et al*., 2003).

Two aspects of the biogenicity problem stand out. First, morphology, in and of itself, has proven inconsistent as an indicator of the biological origin of fossil-like objects. Indeed, on the basis solely of their "biologic-like" morphology, scores of different types of minute non-biologic objects, both of mineralic and of carbonaceous composition, have mistakenly been interpreted to be Precambrian microfossils, including many that have been formally named and are thus archived in the paleobiologic literature (for extensive tabulations, see Hofmann and Schopf, 1983; Schopf and Walter, 1983; Mendelson and Schopf, 1992). Second, the fidelity of preservation of such microscopic objects, a function largely of the geological history of the rocks in which they occur, can decisively influence their interpretation. Thus, even for authentic organic-walled fossils, establishment of biogenicity can be difficult in metamorphosed rock units in which identifiable biological morphology has become all but undecipherable as the "cooked" fossils have deteriorated and their originally amber or brownish-amber carbonaceous cell walls have been converted to blackened, charred, more or less nondescript bits and pieces (Schopf, 1993, 1999a). As is well illustrated by the study of Knoll *et al*. (1988), who coined the term "Archeanization" to refer to such marked diagenetic degradation, the state of preservation of organic-walled fossils, the geochemical maturity of the carbonaceous matter of which they are composed, is of prime importance to interpretation of their origin. Such difficulties have long been recognized—dating from at least as early as the 1960s (Tyler and Barghoorn, 1963), when active studies of Precambrian fossil microbes were first getting underway (Barghoorn and Schopf, 1965; Barghoorn and Tyler, 1965; Cloud, 1965; Schopf, 1968)—but questions regarding the biogenicity of ancient putative fossils continue to be raised (Brasier *et al*., 2002, 2004).

Ideally, the biogenicity problem could be addressed quite effectively were it possible to demonstrate in objects claimed to be microscopic fossils a one-to-one correlation, at a micron scale, of structurally detailed "biological morphology" with organismically distinctive "biological chemistry." In the real world, however, fossil morphology is never perfectly preserved, and biomolecules are inherently geochemically unstable, so the best one might realistically hope for would be a means by which to spatially correlate, in such putative fossils and at such a scale, *preservable* biological morphology and *geochemically altered* biological chemistry. Though additional criteria would also need to be applied, these two indicators of biogenicity—particularly, if taken together and exhibited by multiple examples of the objects in question—seem paramount among the suite of factors to be considered. Thus, evidence support-

ive of a biogenic interpretation would be provided were chemical data to show that populations of objects characterized morphologically as "cellular microfossils" were composed of carbonaceous matter, as would be expected of organically preserved microorganisms, and would seem all but irrefutable were the data to demonstrate that such carbonaceous matter was unquestionably of biological origin. Such a correlation could prove a linchpin both in paleobiological and in astrobiological research. Not only could it help clarify the nature of various "lifelike" microstructures reported from Precambrian rocks, but it would prove invaluable for interpretation of any such objects detected in non-terrestrial samples, such as those planned to be brought back from Mars. To illustrate the point, it is reasonable to suppose that had such a capability been in place, it could well have proved pivotal to interpretation of the "possible fossil microbes" reported from martian meteorite ALH84001 (McKay *et al*., 1996).

Until recently, however, the organic (*i.e*., carbonaceous) composition of Precambrian microfossils could only be inferred indirectly by paleobiologists, primarily on the bases of the color, texture, and, in some instances, the insolubility in mineral-dissolving acids (HF, HCl) of the objects studied. Indeed, the first direct measurements demonstrating the carbonaceous composition of authentic Precambrian fossils evidently date from 2000: analyses by Raman spectroscopy of cysts of single-celled phytoplankton (acritarchs) preserved by compression in a Neoproterozoic shale (Arouri *et al*., 2000) and ion microprobe analyses of permineralized (petrified) fossils in Paleo- and Neoproterozoic cherts (House *et al*., 2000). These seminal studies were soon followed by Raman and ion microprobe analyses of filamentous possible fossil microbes in a Paleoarchean chert (Ueno *et al*., 2001); Raman imagery of permineralized Paleo- and Neoproterozoic fossil cyanobacteria (Kudryavtsev *et al*., 2001) and of colonial and filamentous putative microfossils in three Paleoarchean chert units (Schopf *et al*., 2002a); and electron microprobe studies of Proterozoic and Phanerozoic organic-walled fossils (Boyce *et al*., 2001).

In comparison with the analytical requirements of and data provided by Raman spectroscopy, however, those of ion and electron microprobe analyses are appreciably more limited. For example, ion microprobe analyses excavate and thus partially destroy the specimens probed, and although both ion and electron microprobe studies can be used to map the two-dimensional spatial distribution of elemental carbon in fossilized organic material, neither can provide data about its molecular structure or geochemical maturity. Moreover, both of these techniques typically require that the specimens analyzed be exposed at the surface of polished petrographic thin sections. This requirement limits their application in studies of especially small, optically difficult to identify, micron- or submicron-sized specimens and of materials having rough topography, such as fossil carbonaceous matter exposed on surfaces of fractured rocks (Kaufman and Xiao, 2003) or flaky particles of kerogen freed from mineral matrices by acid maceration. Similarly, this requirement restricts the use of these techniqes for carbon-mapping to two dimensions only, and prohibits their use for analyses of fossils or particulate carbonaceous matter embedded deeply within petrographic thin sections. In contrast, Raman imagery—the technique on which the present work is centered—is non-intrusive and non-destructive; can be used to analyze minute, micron-sized specimens; is applicable to both organic-walled fossils and particulate carbonaceous sapropel whether embedded within thin sections or freed from a rock matrix by acid maceration; permits one-to-one mapping of cellular morphology and chemical–structural characteristics both in two and in three dimensions; and, importantly, provides insight into the geochemical maturity of the carbonaceous matter analyzed. Versatile and powerful, Raman spectroscopy has been proposed as a prime tool for use in the search for evidence of past or present life on Mars (Ellery and Wynn-Williams, 2003; Wang *et al*., 2003).

Despite the obvious power of Raman imagery, it is not a panacea; ambiguity can arise in the interpretation of the data acquired, especially as applied to problems of Precambrian paleobiology. That ancient carbonaceous matter is assuredly biogenic—*i.e*., that it constitutes "kerogen," a term used here to refer to fossilized carbonaceous matter of established biological origin (*cf*. Pasteris and Wopenka, 2003)—can, of course, be demonstrated by showing that it constitutes the cell walls or other preserved structures of authentic fossils (in which instance it is the mode of occurrence of the carbonaceous matter, not solely its chemical–structural characteristics, that establishes its biogenicity). Thus, kerogen can be identified readily in the richly fossiliferous Protero-

Table 1. Estimated Ages, Sampled Localities, and Metamorphic Grades of the 22 Fossiliferous Cherts Studied, Together with a Listing for Each Unit of Five Indices of Organic Metamorphism Exhibited by the Permineralized Kerogens They Contain: (1) Fidelity of Fossil Preservation; (2) Color of Preserved Microfossils; (3) H/C Ratios (for Kerogens Isolated from Bulk Rock Samples); (4) N/C Ratios (for Kerogens Isolated from Bulk Rock Samples); and (5) RIP Values Calculated from the Raman Point Spectra Shown in Fig. 9, as Discussed in the Text

Geologic unit; locality	*Estimated age (Ma)*[a]	*Metamorphic grade*	*Fidelity of fossil preservation*[b]	*Color of preserved kerogen*[c]	*Bulk kerogen*[d]			
					H/C ratio	*N/C ratio*	*RIP*[e]	*Figures*
Kalkberg Limestone; bedded chert, W of Sharon Springs, central New York state, USA[f]	400	"Low grade"[g]	Good	Brown	Unknown	Unknown	8.5	3a, 4a, 9a
Chichkan Formation; stromatolitic chert, Maly Karatau Mountains, Ayusakan, southern Kazakhstan (PPRG #1473)[h]	650	Laumontite-prehnite-pumpellyite[i]	Excellent	Amber brown	Unknown	Unknown	8.6[j]	3b, 4b, 9b
Min'yar Formation; stromatolitic chert, Zimlin River valley, NE of Bakeyvo Village, Bashkiria, Russia (PPRG #1478)[h]	740	Laumontite-prehnite-pumpellyite[i]	Good	Brown	Unknown	Unknown	8.8	3c, 4c, 9c
Skillogalee Dolomite; stromatolitic chert, Peake and Denison Ranges, Lake Eyre North, South Australia (PPRG #1283)[h]	770	Lower greenschist[k]	Fair	Brownish-black	0.22 (n = 8) (0.10–0.33)	0.007 (n = 5) (0.005–0.011)	3.9	3d, 4d, 9d
River Wakefield Subgroup; bedded chert, SW of Carrieton, South Australia (PPRG #1224)[h]	775	Lower greenschist[k]	Poor	Dark brown	0.44 (n = 3) (0.17–0.82)	0.016 (n = 2) (0.007–0.025)	1.0	3e, 4e, 9e
Auburn Dolomite; bedded chert, W of Leasingham, South Australia (PPRG #1220)[h]	780	Lower greenschist[k]	Poor	Brownish-black	0.17 (n = 1) (0.17)	0.010 (n = 1) (0.010)	1.5	3f, 4f, 9f
Bambuí Group; stromatolitic chert, Fazenda Funil, NE of Cabeceiras, south-central Brazil[l]	810	"Unmetamorphosed to subgreenschist"[m]	Good	Brown	Unknown	Unknown	6.4	3g, 4g, 9g
Beck Spring Dolomite; stromatolitic chert, Kingston Range, E of Tecopa, eastern California, USA (PPRG #1271)[h]	850	"Slightly to moderately metamorphosed"[n]	Fair	Brown	0.14 (n = 1) (0.14)	0.016 (n = 1) (0.016)	4.4	3h, 4h, 9h
Bitter Springs Formation; stromatolitic chert, Ellery Gap, W of Alice Springs, Northern Territory, Australia (PPRG #1253)[h]	850	Unknown	Excellent	Brown	0.43 (n = 8) (0.10–0.82)	0.029 (n = 3) (0.025–0.032)	9.0	3i, 4i, 9i
Kwagunt Formation; pisolitic chert, Nankoweap Butte, Grand Canyon, AZ, USA (PPRG #1357)[h]	850	"Unmetamorphosed"[o]	Good	Amber brown	0.81 (n = 6) (0.69–0.91)	0.025 (n = 6) (0.024–0.031)	7.3	3j, 4j, 9j
Valukhtin Formation; stromatolitic chert, Bolshoy Patom River valley, E of Vitim, Siberia, Russia[p]	1,050	Unknown	Good	Brown	Unknown	Unknown	8.4	3k, 4k, 9k
Allamore Formation; stromatolitic chert, NW of Van Horn, west Texas, USA (PPRG #1360)[h]	1,050	"Lowest greenschist"[q]	Good	Dark brown	0.31 (n = 1) (0.31)	0.015 (n = 1) (0.015)	6.7	3l, 4l, 9l

Wumishan Formation; stromatolitic chert, Mopangyu Village, NE of Jixian, northeastern China (PPRG #1435)[h]	1,325	Essentially unmetamorphosed[r]	Good	Amber brown	0.54 (n = 1) (0.54)	0.031 (n = 1) (0.031)	7.4	3m, 4m, 9m
Yangzhuang Formation; bedded chert, Xiaying Village, NE of Jixian, northeastern China (PPRG 2148)[h]	1,350	Essentially unmetamorphosed[r]	Good	Amber brown	0.49 (n = 1) (0.49)	0.026 (n = 1) 0.026	8.1	3n, 4n, 9n
Bungle Bungle Dolomite; stromatolitic chert, Dixon Range region, northeastern Western Australia (PPRG #0159)[s]	1,364	Unknown	Good	Dark brown	0.37 (n = 7) (0.26–0.45)	0.024 (n = 7) (0.010–0.043)	7.5	3o, 4o, 9o
Dismal Lakes Group; stromatolitic chert, W of Dismal Lakes, Northwest Territories, Canada (PPRG #2358)[h]	1,400	Unknown	Good	Brown	0.67 (n = 1) (0.67)	0.015 (n = 1) (0.015)	7.4	3p, 4p, 9p
Gaoyuzhuang Formation; stromatolitic chert, Sangshuan School, NE of Jixian, northeastern China (PPRG #2123)[h]	1,425	Essentially unmetamorphosed[r]	Excellent	Dark brown	0.45 (n = 2) (0.38–0.52)	0.014 (n = 2) (0.012–0.016)	8.5	3q, 4q, 9q
Paradise Creek Formation; stromatolitic chert, Paradise Creek, Queensland, Australia (PPRG #1260)[h,t]	1,650	Unknown	Not detected	Brown[c]	0.20 (n = 1) (0.20)	Unknown	5.3	9u
Vempalle Formation; stromatolitic chert, Bramanapalle Asbestos Mine, Andhra Pradesh, India (PPRG #1308)[h]	1,700	Subgreenschist[u,v]	Fair	Dark brown	Unknown	Unknown	5.7	3r, 4r, 9r
Duck Creek Dolomite; bedded chert, Wyloo region, northwestern Western Australia (PPRG #0060)[h]	2,000	Pumpellyite-epidote[w]	Poor	Brownish-black	0.23 (n = 2) (0.14–0.32)	0.008 (n = 2) (0.005–0.011)	3.4	3s, 4s, 9s
Gunflint Formation; stromatolitic chert, W of Schreiber, southern Ontario, Canada (PPRG #1289)[h]	2,090	Subgreenschist[w]	Good	Brown	0.40 (n = 7) (0.10–0.61)	0.018 (n = 6) (0.005–0.022)	8.8	3t, 4t, 9t
McLeary Formation; stromatolitic chert, Belcher Islands, Northwest Territories, Canada (PPRG # 0447)[s,x]	2,100	Subgreenschist[w]	Not detected	Brown[c]	0.26 (n = 1) (0.26)	0.013 (n = 1) (0.013)	5.8	9v

References are as follows: [f]Wicander and Schopf (1974); [g]Marshak and Engelder (1985); [h]Moore and Schopf (1992); [i]Sobolev *et al*. (1982); [k]Ambrose *et al*. (1981) and Preiss (1987); [l]Fairchild *et al*. (1996); [m]Marshak and Alkmim (1989); [n]Carlisle *et al*. (1980); [o]Dehler *et al*. (2001); [p]Schopf *et al*. (1977); [q]Bickford *et al*. (2000); [r]Wang and Qiao (1987); [s]Walter *et al*. (1983); [t]Licari *et al*. (1969); [u]Riding and Sharma (1998); [v]Crawford and Compston (1973); [w]Hayes *et al*. (1983); [x]Hofmann (1976).

[a]The age listed for the Bambuí Group is that estimated by Fairchild *et al*. (1996); for the Valukhtin Formation, by Schopf *et al*. (1977); for the Duck Creek Dolomite, by Knoll and Barghoorn (1976); and for the McLeary Formation, by Hofmann (1976). Except for these ages and that of the Lower Devonian Kalkberg Limestone, ages listed are those estimated by Moore and Schopf (1992).

[b]Evaluation (by J.W.S.) of fidelity of preservation of fossils in the thin sections containing the kerogens analyzed by Raman spectroscopy.

[c]As shown in Figs. 3, 4, and 12, colors of kerogens in fossiliferous cherts of the Paradise Creek (Licari *et al*., 1969) and McLeary (Hofmann, 1976) Formations were determined on wispy clouds of finely divided particulate kerogen, not that comprising microfossils.

[d]Average value and number and range of measurements summarized by Strauss and Moore (1992).

[e]For explanation of the RIP, see text and Fig. 9.

[j]Average of measurements of 135 fossils (Fig. 11).

zoic (<2,500-Ma-old) Precambrian (Mendelson and Schopf, 1992) where Raman imagery has shown such carbonaceous matter to comprise the permineralized cellular remnants of stromatolite-building microorganisms (Kudryavtsev *et al*., 2001; Schopf *et al*., 2002a), kerogen that in relatively unmetamorphosed deposits exhibits what we regard to be an identifying Raman signature (Kudryavtsev *et al*., 2001).

However, in the older, Archean (>2,500-Ma-old) Precambrian, establishment of the biological origin of preserved carbonaceous matter (*i.e*., that it assuredly constitutes "kerogen") is not as straightforward. In comparison with the fossil record of the Proterozoic, that of the Archean is minuscule (Schopf and Walter, 1983; Schopf, 1992a, 2004; Altermann, 2001). And not only are relatively few Archean-age fossils available for study, but all of those that are known are poorly preserved, hosted by rocks that have experienced at least low-grade (most commonly, greenschist facies) metamorphism that, by producing incipient graphitization, has obscured the distinctive Raman signature exhibited by less altered carbonaceous matter (Kudryavtsev *et al*., 2001). Moreover, especially ancient Archean units may arguably be expected to harbor carbonaceous substances of entirely non-biological origin, derived from organic matter like that present on the pre-life Earth. Yet all such carbonaceous matter-containing units now known have been metamorphosed, some severely [such as those of the ~3,800-Ma-old Isua Supracrustal Group, to amphibolite facies (Bridgwater *et al*., 1981; Nutman *et al*., 1984)]. And since geochemical maturation of almost all naturally occurring organic materials, whether of biological or solely abiotic origin, can be expected to give rise to essentially the same set of resultant stable products—interlinked polycyclic aromatic hydrocarbons (PAHs) that under geological conditions can become increasingly carbonized and graphitized and, ultimately, converted to crystalline graphite (*e.g*., Durand, 1980; Pasteris and Wopenka, 1991; Wopenka and Pasteris, 1993)—Raman spectroscopy of mature carbonaceous matter cannot, by itself, provide definitive evidence of biogenicity. Combined with data from other sources, such as those from morphometric studies of populations of fossil microorganisms (Schopf, 1992b, 1999a), carbon isotopic analyses of preserved carbonaceous matter (Hayes *et al*., 1983; Strauss and Moore, 1992; Strauss *et al*., 1992a,b; House *et al*., 2000; Kaufman and Xiao, 2003), and/or intramolecular isotopic measurements on particular organic constituents (Hayes, 2004), Raman analyses can play a role in addressing this problem (Ueno *et al*., 2001; Schopf *et al*., 2002a; Tice *et al*., 2004), but only as one of several mutually reinforcing lines of evidence.

Thus, by themselves, Raman spectra of geochemically mature organic matter can establish only its carbonaceous composition, not its biological origin. In the present study, however, uncertainty regarding the biogenicity of the organic matter investigated can be set aside since the results reported here are based entirely on well-documented submetamorphosed or little metamorphosed (lower greenschist facies) fossil-bearing deposits of post-Archean age in which Raman imagery directly demonstrates that the carbonaceous matter analyzed comprises the cell walls or other preserved structures of authentic microscopic fossils. Further, carbon isotopic analyses establish that the carbonaceous components of all of the units for which such data are available fall well within the range typical of biologically produced organic matter. In addition, all of the units date from less

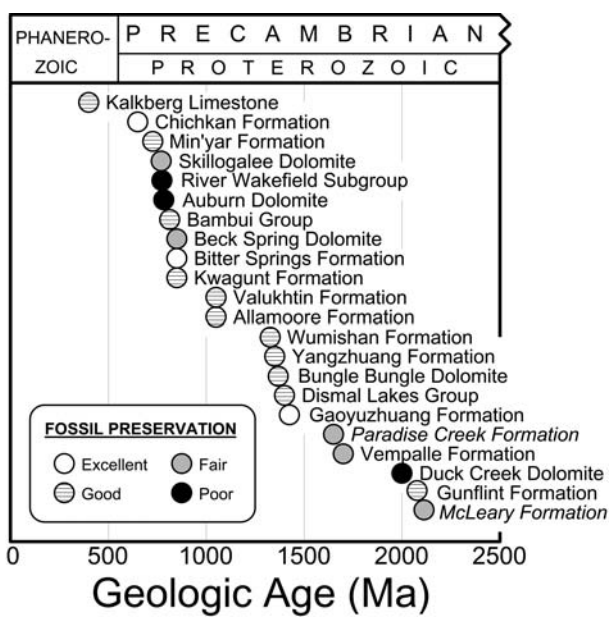

FIG. 1. Temporal distribution of the 22 fossiliferous cherts analyzed, showing that the fidelity of fossil preservation is not closely correlated with the geologic age of the fossil-bearing units. Fidelity of fossil preservation for the Paradise Creek and McLeary Formations (listed in italics), for which fossils were not detected in the thin sections studied here, is estimated on the basis of published photomicrographs (Licari *et al*., 1969; Hofmann, 1976).

than 2,320 Ma ago when the advent of a stable oxygen-containing atmosphere (Bekker *et al*., 2004) would have rendered Miller/Urey-type organic syntheses inoperable, making it quite unlikely that any of these deposits contains non-biological organic matter derived from such reactions.

By focusing our use of Raman imagery on the study of fossil microorganisms and associated organic detritus permineralized in 22 geologic units of essentially the same lithology (*viz*., fine-grained cherts), but of disparate ages (spanning a range of ~1,600 Ma, from Paleoproterozoic to Devonian) and differing low-grade metamorphic histories, we show that there is a geochemical continuum that extends from the kerogenous constituents of relatively "well-preserved" to

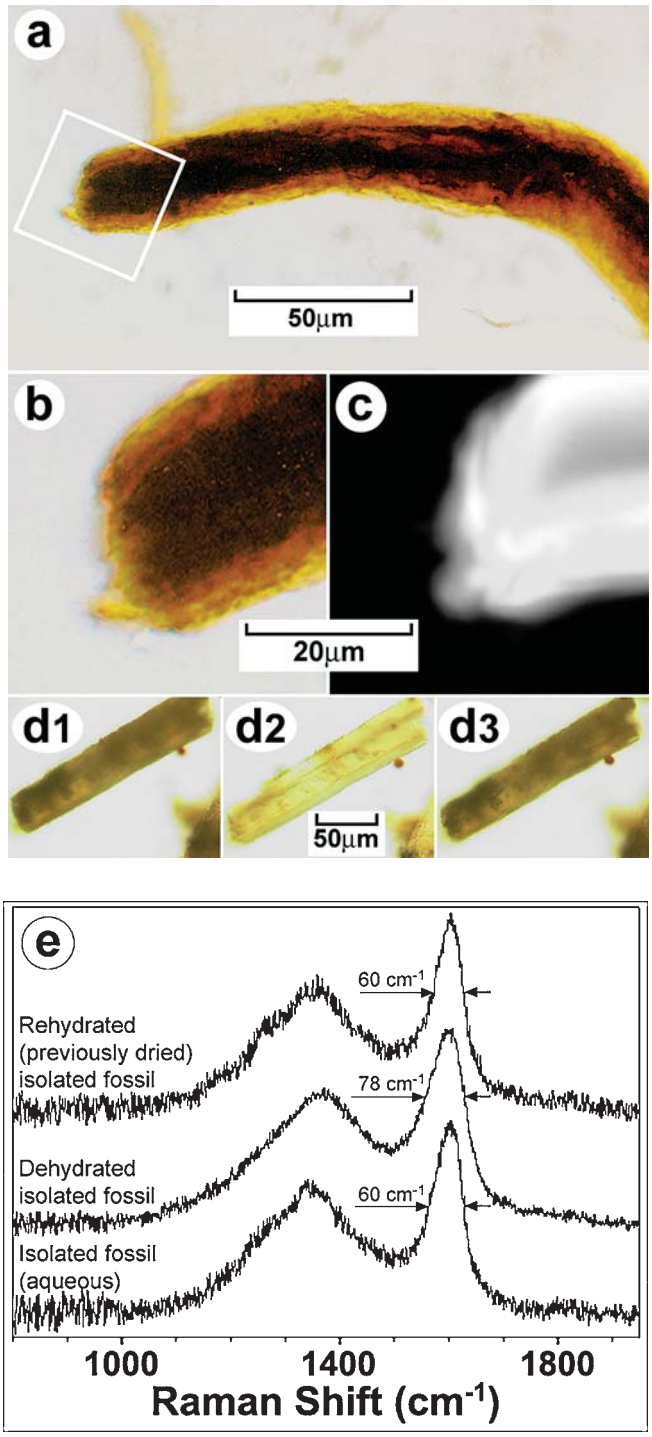

FIG. 2. Optical photomicrographs, Raman spectra, and a Raman image of *Schizothrichites ordoviciensis*, a filamentous sheath-enclosed oscillatoriacean cyanobacterium preserved by permineralization in Ordovician (Tremadocian, ~475-Ma-old) chert of the Holy Cross Mountains of Poland (Starmach, 1963; Schopf, 1974), isolated from the chert by HF maceration and photographed in a glycerine mount (a–c), in water (d2), and in a preparation dehydrated in air (d1 and d3). a: Optical photomicrograph of a specimen in which the white rectangle denotes the area analyzed by Raman imagery. b and c: Digitized optical image (b) and Raman image (c) of the terminal portion of the fossil shown in (a). d: Sequential digitized images of an isolated specimen photographed first (d1) in a dehydrated preparation, then (d2) hydrated in water, and then (d3) again dehydrated, showing that the color of the organically preserved fossil varies reversibly during the dehydration–hydration–dehydration sequence from darker/more intense to lighter/less intense to darker/more intense. **e:** Raman spectra of the specimen shown in (d): (bottom) in water, before dehydration (having an RIP value of 9.3); (middle) after dehydration (RIP = 9.6); and (top) after rehydration (RIP = 9.3). In all spectra, the prominent vibrational bands at ~1,350 cm^{-1} ("D" band) and ~1,600 cm^{-1} ("G" band) establish the carbonaceous (kerogenous) composition of the fossils. Arrows in (e) indicate the measured full width at half-maximum of the "G" band, showing that changes in the width of this band during the hydration–dehydration–rehydration sequence are, like those of the color of the fossils, largely reversible.

"poorly preserved" microscopic fossils. This continuum is consistent with (1) the mineral-based metamorphic facies of the host rock (where known, albeit imprecisely) and is evidenced not only by (2) the relative fidelity of structural preservation of the fossils in the various units and (3) systematic differences among the Raman spectra of their carbonaceous components, but by (4) the optically quantifiable differing colors (ranging from amber brown to black) of organic matter preserved in the various units as well as by differences among the (5) H/C and (6) N/C ratios measured in bulk samples of kerogens isolated from more than two-thirds of the units investigated.

The present work is, in essence, a "proof of concept" paper. Our aim is to demonstrate that Raman imagery, paleobiologically a novel use of Raman spectroscopy (Kudryavtsev *et al*., 2001; Schopf *et al*., 2002a), is broadly applicable to the study of ancient carbonaceous matter, a technique that not only can establish a one-to-one spatial correlation between the optically discernible morphology and chemical–structural characteristics of the kerogen comprising organic-walled fossils and associated sapropelic debris, but also can yield useful insight into the geochemical maturity of the carbonaceous materials analyzed. Of obvious relevance to assessment of the biogenicity of ancient microscopic fossils, such analyses have been (Ueno *et al*., 2001; Schopf *et al*., 2002a) and will continue to be applied to putative microfossils discovered in Archean terrains, but for sound interpretation of the results obtained, the efficacy of the concept and the bases of its application need first to be established on younger fossil assemblages of unquestionable biologic origin.

MATERIALS AND METHODS

Geologic units studied

Table 1 lists the 22 geologic units and localities from which were obtained the analyzed fossil-bearing cherts (predominately stromatolitic and all relatively fine-grained, composed typically of interlocking mosaics of ~2–10-μm-sized grains of cryptocrystalline quartz), as well as the mineral-based metamorphic grade of the various units and five other indices of the degree of maturity of their preserved organics: (1) fidelity of fossil preservation; (2) kerogen color; (3) H/C and (4) N/C ratios measured in bulk samples of isolated kerogens; and (5) the Raman Index of Preservation (RIP), a Raman-based estimate of the geochemical maturity of the kerogens analyzed, newly introduced here. Figure 1 summarizes the temporal distribution of the 22 units studied.

Preparation techniques

With the exception of particulate kerogens and microbial fossils analyzed in aqueous or dehydrated preparations of HF-resistant residues (Fig.

FIG. 3. Transmitted light photomicrographs showing kerogenous microscopic fossils preserved by permineralization in 22 fine-grained chert units of Devonian (a) and diverse Precambrian (Table 1) ages. Some panels show photomontages, necessitated by the three-dimensional preservation of the permineralized microbes; rectangles in each part denote the areas for which Raman images are shown in Fig. 4. **a:** *Multiplicisphaeridium* sp., a spiny (acanthomorph) acritarch (Kalkberg Limestone, Lower Devonian, ~400 Ma old, New York) (Wicander and Schopf, 1974). **b:** An unnamed oscillatoriacean (*Lyngbya*-like) tubular sheath (Chichkan Formation, ~650 Ma old, southern Kazakhstan) (Schopf and Sovietov, 1976; Schopf *et al*., 1977). **c:** An unnamed cylindrical filament, probably the degraded trichome of an oscillatoriacean cyanobacterium (Min'yar Formation, ~740 Ma old, central Russia) (Schopf *et al*., 1977; Nyberg and Schopf, 1984). **d:** An unnamed cylindrical filament, probably the degraded trichome of an oscillatoriacean cyanobacterium (Skillogalee Dolomite, ~770 Ma old, South Australia) (Schopf and Fairchild, 1973; Schopf, 1977; Preiss, 1987; Schopf, 1992c). **e:** *Polybessurus bipartitus*, the asymmetrically laminated stalk secreted by a *Solentia*-like pleurocapsacean cyanobacterium (River Wakefield Subgroup, ~775 Ma old, South Australia) (Schopf, J.W., 1975, 1977, 1992c). **f:** An unnamed ellipsoidal unicell (Auburn Dolomite, ~780 Ma old, South Australia) (Schopf, J.W., 1975, 1992c). **g:** An unnamed spheroidal unicell (Bambuí Group, ~810 Ma old, north-central Brazil) (Fairchild *et al*., 1996). **h:** *Beckspringia communis*, the degraded cellular trichome of an oscillatoriacean cyanobacterium (Beck Spring Dolomite, ~850 Ma old, California) (Licari, 1978). **i:** *Glenobotrydion aenigmatis*, a chroococcacean cyanobacterium (Bitter Springs Formation, ~850 Ma old, central Australia) (Schopf, 1968; Schopf and Blacic, 1971). **j:** An unnamed ensheathed chroococcacean cyanobacterium (Kwagunt Formation, ~850 Ma old, Arizona) (Schopf *et al*., 1973; Bloeser *et al*., 1977). **k:** An unnamed cellular trichome of an oscillatoriacean cyanobacterium (Valukhtin Formation, ~1,050 Ma old, Siberia, Russia) (Schopf *et al*., 1977). **l:** An unnamed spheroidal unicell (Allamoore Formation, ~1,050 Ma old, Texas) (Nyberg and Schopf, 1981). **m:** *Eomycetopsis robusta*, the tubular sheath of an oscillatoriacean cyanobacterium (Wumishan Formation, ~1,325 Ma old, northeastern China) (Zhang, 1985).

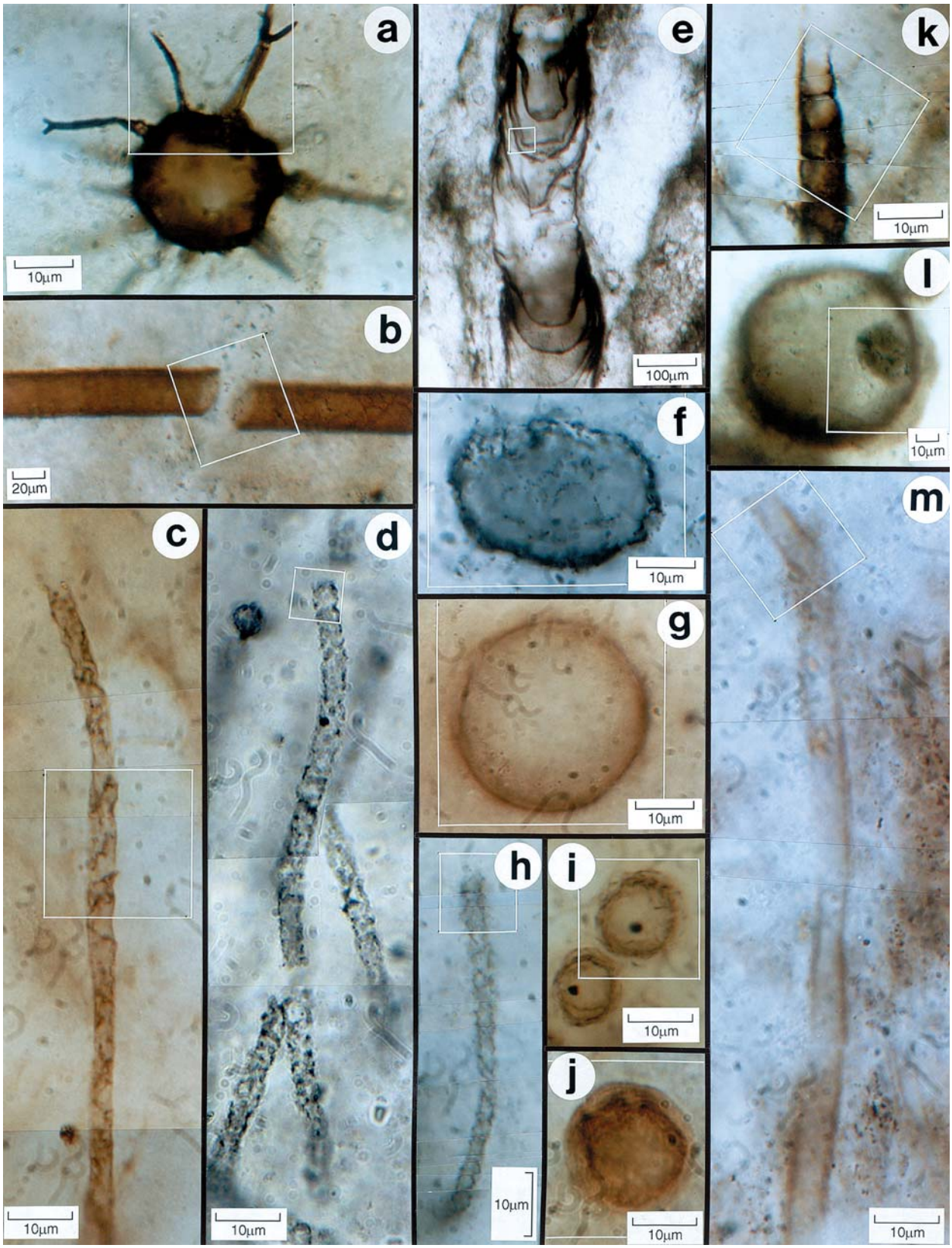
a
10μm
b
20μm
c
10μm
d
10μm
e
100μm
f
10μm
g
10μm
h
10μm
i
10μm
j
10μm
k
10μm
l
10μm
m
10μm

FIG. 3a–m.

2), all fossils were studied in unpolished petrographic thin sections (finished by use of a slurry of 600 grit carborundum, and covered by a thin veneer of Type B non-drying microscopy immersion oil; R.P. Cargille Laboratories, Inc., Cedar Grove, NJ). The analyzed specimens were located by optical microscopy and photographed in transmitted white light by use of a Leitz (New York, NY) Orthoplan 2 automatic photomicroscope and Ektachrome 64T professional film (Eastman Kodak, Rochester, NY) (Fig. 3).

Fossil assemblages investigated

The Raman analyses reported here are based on studies of authentic microfossils, cellularly permineralized Proterozoic and Phanerozoic microorganisms preserved in well-documented, biologically diverse, fossil communities. As is noted in Table 1, the 22 fossiliferous chert units studied include one that is pisolitic (Kwagunt Formation); five that are bedded (Kalkberg Limestone; Auburn and Duck Creek Dolomites; Yangzhuang Formation; and River Wakefield Subgroup); and 16 that are stromatolitic, ranging from flat-laminated (*e.g.*, Bitter Springs, Min'yar, and Wumishan Formations) to domical (*e.g.*, Skillogalee and Beck Spring Dolomites and Gunflint Formation) or conical (Chichkan and Gaoyuzhuang Formations). Among these are many that contain microbial communities that form the basis of current understanding of the early history of life—"classic" fossil assemblages, such as those of the Gunflint and Bitter Springs cherts, described in detail in the 1960s (Barghoorn and Schopf, 1965; Barghoorn and Tyler, 1965; Cloud, 1965; Schopf, 1968), as well as those from other units that have received extensive paleobiologic investigation (*e.g.*, Skillogalee, Beck Spring, Bungle Bungle, and Duck Creek Dolomites and the Min'yar, Allamoore, Paradise Creek, and McLeary Formations). The relevant paleontological literature for each of the fossiliferous cherts here studied is referenced in Table 1 and in the legend to Fig. 3. Each of the units contains thousands of permineralized fossil microbes of known biological affinities and distinct morphologies, typically single and paired coccoidal cells; colonies of spheroidal or ellipsoidal cells; narrow to broad cellular filaments; and cylindrical, tubular, filamentous sheaths. Some of the assemblages are augmented by microbial fossils of more complex form (*e.g.*, *Polybessurus* from the River Wakefield Subgroup; Figs. 3e and 4e) or of less certain phylogenetic relations (*e.g.*, *Eosphaera* from the Gunflint Formation; Figs. 3t and 4t). Importantly, even the most "poorly preserved" (most graphitized) assemblage here investigated—that permineralized in ~775-Ma-old bedded cherts of the River Wakefield Subgroup of South Australia—is morphologically and biologically diverse, containing solitary microbial spheroidal unicells (Fig. 5d, e, and j); colonial coccoidal microbes, many surrounded by well-defined, originally mucilagenous, envelopes (Fig. 5a–c, g, l, and m); tubular, cyanobacterial, filamentous sheaths (Fig. 5f, h, i, and k); and hundreds of specimens of the stalked pleurocapsacean cyanobacterium *Polybessurus* (Figs. 3e, 4e, and cover of this issue of *Astrobiology*) (Schopf, J.W., 1975, 1977, 1992c). All specimens for which data are reported here are housed in the Raman Spectroscopy Sample Collections of the Institute of Geophysics & Planetary Physics Center for the Study of Evolution and the Origin of Life at UCLA (Los Angeles, CA).

Heating experiments

To simulate the thermal alteration of organic matter that accompanies the low-temperature (diagenic/catagenic/metagenic) maturation of the kerogens studied, a series of heating experiments, similar in aim to those performed by Marshall *et*

FIG. 3 (continued). **n:** An unnamed spheroidal unicell (Yangzhuang Formation, ~1,350 Ma old, northeastern China) (Xing and Liu, 1973). **o:** *E. robusta*, the tubular sheath of an oscillatoriacean cyanobacterium (Bungle Bungle Dolomite, ~1,364 Ma old, Western Australia) (Diver, 1974; Hofmann and Schopf, 1983). **p:** *Oscillatoriopsis curta*, the cellular trichome of an oscillatoriacean cyanobacterium (Dismal Lakes Group, ~1,400 Ma old, Northwest Territories, Canada) (Schopf, J.W., 1975; Horodyski and Donaldson, 1980, 1983). **q:** *Eomycetopsis filiformis*, the tubular sheath of a oscillatoriacean cyanobacterium (Gaoyuzhuang Formation, ~1,425 Ma old, northeastern China) (Zhang, 1981; Schopf *et al*., 1984). **r:** An unnamed flattened sheath of an oscillatoriacean cyanobacterium (Vempalle Formation, ~1,700 Ma old, south-central India) (Schopf and Prasad, 1978). **s:** An unnamed cylindrical filament, probably the degraded trichome of an oscillatoriacean cyanobacterium (Duck Creek Dolomite, ~2,000 Ma old, Western Australia) (Knoll and Barghoorn, 1976; Hofmann and Schopf, 1983; Knoll *et al*., 1988). **t:** *Eosphaera tyleri*, a spheroidal presumably prokaryotic microfossil of uncertain systematic position (Gunflint Formation, ~2,090 Ma old, Ontario, Canada) (Barghoorn and Tyler, 1965; Schopf, 1977; Hofmann and Schopf, 1983).

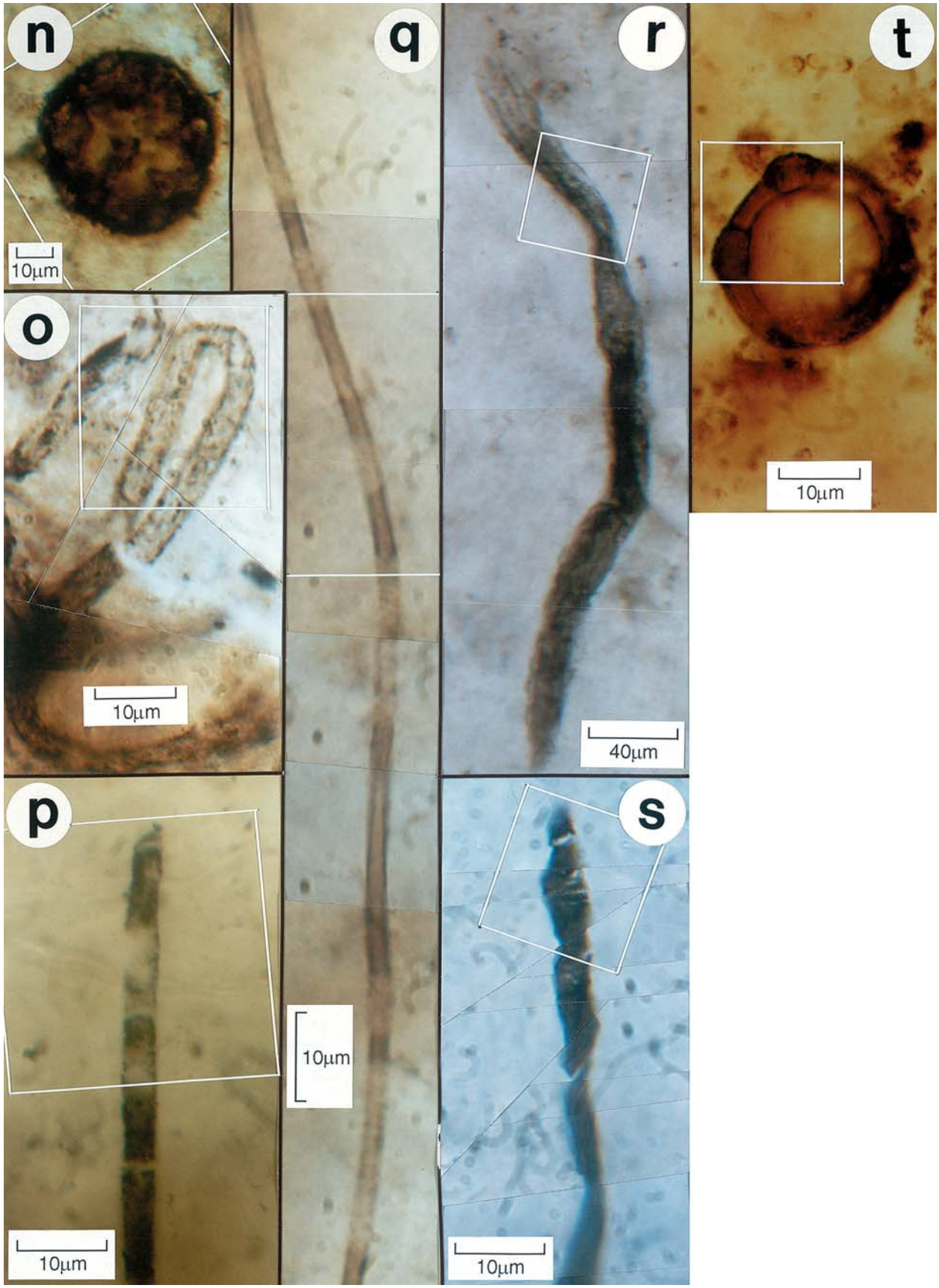

FIG. 3n–t.

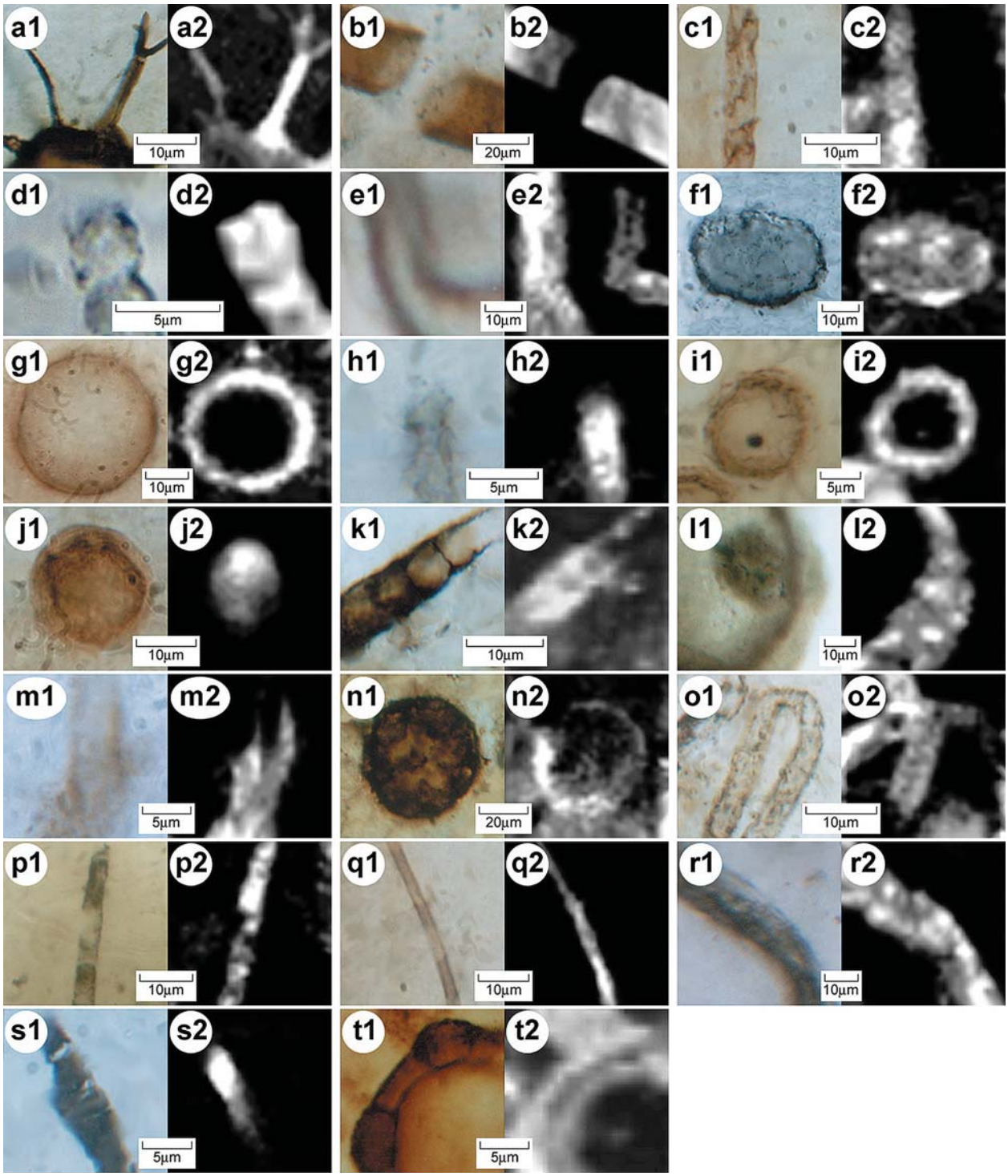

FIG. 4. Areas of the fossils outlined by white rectangles in Fig. 3, shown here in digitized images (denoted by suffix "1") and Raman images of the same areas (denoted by suffix "2"), with the prefix letters indicating the geologic source of the fossils as indicated in Figs. 3 and 9.

al. (2001) on acid-macerated pulverized conodonts, were conducted on rock slices containing particularly well-preserved microscopic fossils (from the Bitter Springs and Chichkan Formations; Table 2). Fossils were located by light microscopy in petrographic thin sections that had been cemented onto an underlying glass microscope slide by an acetone-soluble cement. To facilitate relocation of the

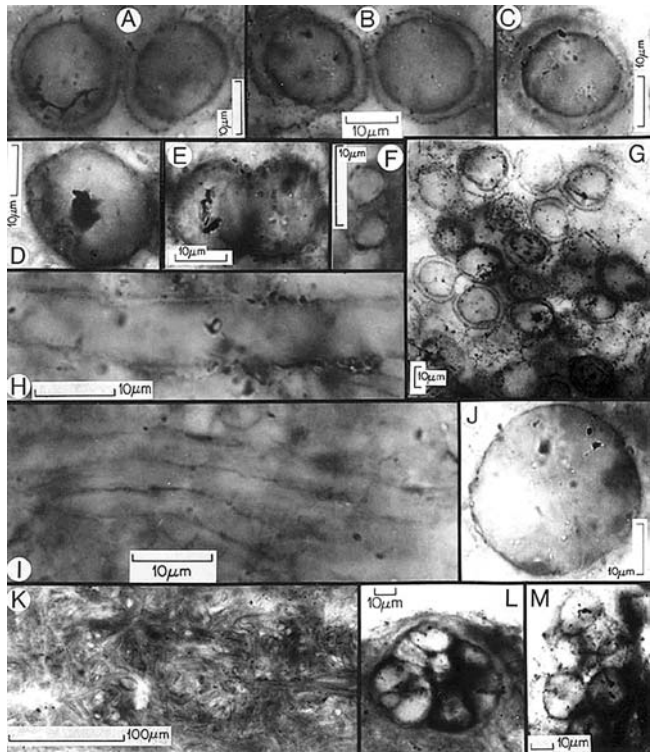

FIG. 5. Optical photomicrographs showing relatively poorly preserved (Fig. 1) fossils of the River Wakefield Subgroup (~775 Ma old, Port Augusta region, South Australia) (Schopf, J.W., 1975, 1977, 1992c), composed of kerogen that is the geochemically most altered (Figs. 7 and 9 and Table 2) of those studied here. A–C and **G:** Unnamed sheath-enclosed colonial unicells. **D, E,** and **J:** Unnamed spheroidal unicells. **F, H,** and **I:** Unnamed tubular microbial sheaths shown in transverse (F) and longitudinal (H and I) sections. **K:** Unnamed tubular sheaths comprising an entangled stratiform mat. **L** and **M:** Unnamed colonial coccoid cells.

fossils after heating, the upper surface of each thin section was then partially cored by use of a Sonatron sonic disintegrator drill (Kenyon Electronics, Jersey City, NJ) to produce 3–mm-diameter circles that enclosed the fossil-containing areas. The cementing medium was then dissolved in acetone, and the fossil-bearing slices were cleaned of any adhering organic materials in a soxhlet extractor for 24 h, using a 1:1 (vol/vol) benzene/methanol solution. The cleaned slices were heated progressively in a tube furnace (Lindberg/Blue M, Thermal Product Solutions, Williamsport, PA) for 2-h periods under anoxic conditions (under a continuous flow of argon at a rate of ~0.04 m^3/h) at increments of 50°C, from 200 to 800°C; at increments of 100°C, from 800 to 1,000°C; and at an increment of 200°C, from 1,000 to 1,200°C. After heating, the slices were allowed to cool under argon to room temperature, typically over a 10–12–h period. Raman spectra of the heat-treated fossils were acquired at each step of such sequences. Figure 6a shows an example of the results obtained.

Raman spectroscopy

Raman spectra. The laser-Raman spectroscopic data presented here were obtained by use of a Dilor XY (formerly, Instruments S.A.; now JY Horiba, Edison, NJ) 0.8-m triple-stage system having macro-Raman, micro-Raman, and confocal line-scan Raman imaging capabilities. All three gratings of the system (each having a groove density of 1,200 grooves mm^{-1}) were holographic, and the spectrograph was typically set in a subtractive configuration. A liquid nitrogen-cooled charge-coupled device, having 2,000 × 800 pixels (each 15 × 15 μm in size), was used to detect especially weak Raman signals. This system permitted acquisition both of individual point spectra and of Raman images that display the two-dimensional spatial distribution of chemical–structural components. Due to the confocal capability of the system, use of a 100× objective (having an extended working distance of 3.4 mm, a numerical aperture of 0.8, and not requiring immersion oil) to obtain the Raman data reported here provided a planar resolution of <1 μm and, by use of a confocal hole size of 150–200 μm, a vertical resolution of 1–3 μm. A Coherent® (Santa Clara, CA) krypton ion laser equipped with appropriate optics provided laser wavelengths ranging from blue to infrared, of which 531 nm (in the green portion of the visible spectrum) and 476 nm (in the blue portion of the spectrum) were used. Spectra acquired at each wavelength were normalized to the correspond-

TABLE 2. THE 22 FOSSILIFEROUS CHERTS STUDIED, SHOWING THE CORRELATION BETWEEN THE RIP VALUES OF THEIR ANALYZED KEROGENS AND FOUR OTHER INDICES OF ORGANIC METAMORPHISM: (1) THE FIDELITY OF FOSSIL PRESERVATION; (2) THE COLOR OF PRESERVED MICROFOSSILS; AND, FOR KEROGENS ISOLATED FROM BULK ROCK SAMPLES, THEIR APPROXIMATE (3) H/C AND (4) N/C RATIOS

Geologic unit	*RIP*[a]	*Fidelity of fossil preservation*[b]	*Color of preserved fossils*[c]	*Bulk kerogen*[d]		*Figures*
				H/C ratio	*N/C ratio*	
Bitter Springs Formation	9.0	Excellent	Brown (2.0)	~0.50[e]	~0.030	3i, 4i, 9i
Gunflint Formation	8.8	Good	Brown (1.9)	~0.45[e]	~0.020[f]	3t, 4t, 9t
Chichkan Formation	8.8[g]	Excellent	Amber brown (2.6)	Unknown	Unknown	3b, 4b, 9b
Min'yar Formation	8.6	Good	Brown (1.8)	Unknown	Unknown	3c, 4c, 9c
Gaoyuzhuang Formation	8.5	Excellent	Dark brown (1.4)	~0.45	~0.015	3q, 4q, 9q
Kalkberg Limestone	8.5	Good	Brown (2.0)	Unknown	Unknown	3a, 4a, 9a
Valukhtin Formation	8.4	Good	Brown (1.5)	Unknown	Unknown	3k, 4k, 9k
Yangzhuang Formation	8.1	Good	Amber brown (3.0)	~0.50	~0.025	3n, 4n, 9n
Bungle Bungle Dolomite	7.5	Good	Dark brown (1.4)	~0.40	~0.025	3o, 4o, 9o
Dismal Lakes Group	7.4	Good	Brown (1.6)	~0.65	~0.015	3p, 4p, 9p
Wumishan Formation	7.4	Good	Amber brown (3.1)	~0.55	~0.030	3m, 4m, 9m
Kwagunt Formation	7.3	Good	Amber brown (2.2)	~0.80	~0.025	3j, 4j, 9j
Allamoore Formation	6.7	Good	Dark brown (1.2)	~0.30	~0.015	3l, 4l, 9l
Bambuí Group	6.4	Good	Brown (2.0)	Unknown	Unknown	3g, 4g, 9g
McLeary Formation	5.8	Not detected	Brown (1.9)[c]	~0.25	~0.015	9u
Vempalle Formation	5.7	Fair	Dark brown (1.1)	Unknown	Unknown	3r, 4r, 9r
Paradise Creek Formation	5.3	Not detected	Brown (1.8)[c]	~0.20	Unknown	9v
Beck Springs Dolomite	4.4	Fair	Brown (1.6)	~0.15	~0.015	3h, 4h, 9h
Skillogalee Dolomite	3.9	Fair	Brownish-black (0.9)	~0.20	~0.005	3d, 4d, 9d
Duck Creek Dolomite	3.4	Poor	Brownish-black (0.9)	~0.25	~0.010	3s, 4s, 9s
Auburn Dolomite	1.5	Poor	Brownish-black (0.7)	~0.15	~0.010	3f, 4f, 9f
River Wakefield Subgroup	1.0	Poor	Dark brown (1.1)	~0.15[h]	~0.005[i]	3e, 4e, 9e

[a]For explanation of the RIP, see text and Fig. 9.

[b]Evaluation (by J.W.S.) of fidelity of preservation of fossils in the thin sections containing the kerogens analyzed by Raman spectroscopy.

[c]As shown in Figs. 3, 4, and 12. Values given in parentheses are R/B ratios, as discussed in the text. Colors of kerogens in fossiliferous cherts of the Paradise Creek (Licari *et al*., 1969) and McLeary (Hofmann, 1976) Formations were determined on wispy clouds of finely divided particulate kerogen, not that comprising microfossils.

[d]Approximate average values from Table 1, except for those of cherts from the Bitter Springs and Gunflint Formations and River Wakefield Subgroup (see footnotes e–i).

[e]On the bases of fidelity of fossil preservation, fossil color, N/C ratio, and RIP values, it seems likely that the kerogens analyzed here from cherts of the Bitter Springs and Gunflint Formations are somewhat less dehydrogenated than is indicated by the average value for each unit listed in Table 1. The approximate average H/C ratios listed here have therefore been corrected to exclude anomalously low values [for each unit, one measurement of an H/C ratio of 0.10 (Strauss and Moore, 1992)].

[f]On the bases of fidelity of fossil preservation, fossil color, H/C ratio, and RIP value, it seems likely that the kerogen analyzed here from chert of the Gunflint Formation is somewhat less denitrogenated than is indicated by the average value for this unit listed in Table 1. The approximate average N/C ratio listed here has therefore been corrected to exclude one anomalously low value [of 0.005 (Strauss and Moore, 1992)].

[g]Average of measurements of 135 fossils (Fig. 11).

[h]On the bases of fidelity of fossil preservation, fossil color, N/C ratio, and RIP value, it seems likely that the kerogen analyzed here from chert of the River Wakefield Subgroup is more dehydrogenated than is indicated by the average value for this unit listed in Table 1. The approximate average H/C ratio here has therefore been corrected to exclude two anomalously high values [of 0.33 and 0.82 (Strauss and Moore, 1992)].

[i]On the bases of fidelity of fossil preservation, fossil color, H/C ratio, and RIP value, it seems likely that the kerogen analyzed here from chert of the River Wakefield Subgroup is more denitrogenated than is indicated by the average value for this unit listed in Table 1. The approximate N/C ratio listed here has therefore been corrected to exclude one anomalously high value [of 0.025 (Strauss and Moore, 1992)].

ing spectral response function of the system. Except for Raman spectra spanning the range from 375 to 3,470 cm^{-1} (Fig. 7), all point spectra and Raman images shown here were acquired in the carbon first-order region by use of a single spectral window centered at 1,400 cm^{-1} that for laser excitation at 531 nm provided coverage from 930 to 1,840 cm^{-1}, and for excitation at 476 nm, from

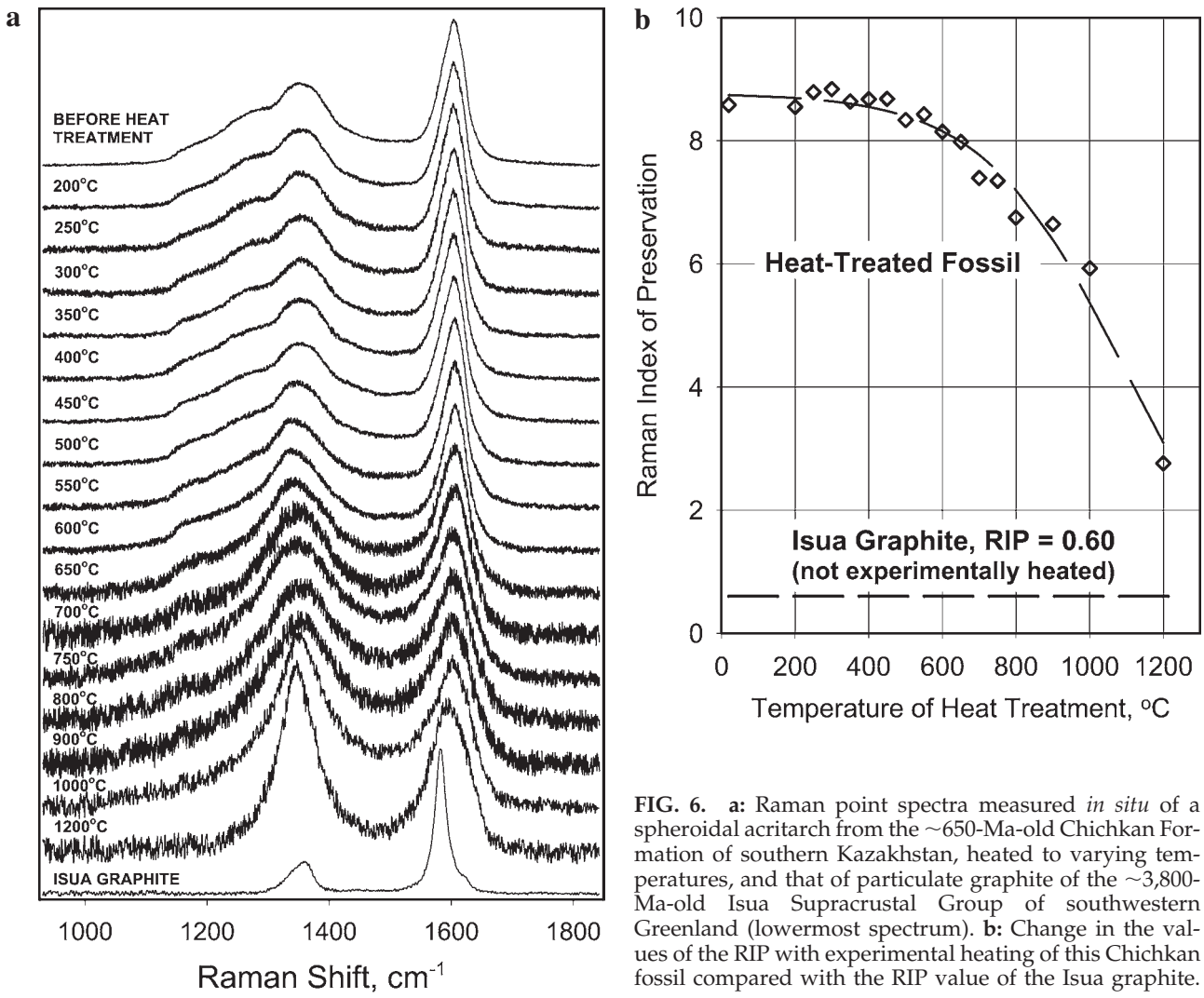

FIG. 6. **a:** Raman point spectra measured *in situ* of a spheroidal acritarch from the ~650-Ma-old Chichkan Formation of southern Kazakhstan, heated to varying temperatures, and that of particulate graphite of the ~3,800-Ma-old Isua Supracrustal Group of southwestern Greenland (lowermost spectrum). **b:** Change in the values of the RIP with experimental heating of this Chichkan fossil compared with the RIP value of the Isua graphite.

800 to 1,960 cm^{-1}. Spectra shown in Fig. 7 were measured in parts of four spectral windows (centered at 1,000, 1,400, 2,200, and 3,000 cm^{-1}, respectively), with the data acquired being subsequently "pasted" together into a single spectrum. Despite concerted study, no evidence of the effects of polarization was detected in the spectra of any of the materials here analyzed.

For all Raman spectra, the typical laser power was <8 mW over a ~1-μm spot, an instrumental configuration well below the threshold that results in radiation damage to such specimens (Schopf *et al*., 2002a). For analysis, specimens were centered in the path of the laser beam projected through an Olympus (Melville, NY) BX40 microscope. To enhance the optical image of specimens in unpolished thin sections, the area analyzed was covered by a thin veneer (~1 μm thick) of Type B non-drying microscopy immersion oil, the presence of which has been shown to have no appreciable effect on the Raman spectra acquired (Schopf *et al*., 2002a). Spectra were obtained from fossils and particulate kerogens situated in such sections over a range of depths, from being at or near the upper surface of a thin section to being embedded at depths as great as ~65 μm.

Raman imaging. To acquire Raman images (Figs. 2 and 4), a rectangular area enclosing a part of a fossil was selected for imaging; the backscattered Raman spectra obtained within such rectangles were collected through the optical system described above, along micrometer-resolution scan lines; and the *x-y* registrations of the data obtained were then automatically recorded to provide a pixel-assigned array of spectral elements ("spexels"). A typical Raman image was composed of 25 × 25 spectral elements, each analyzed

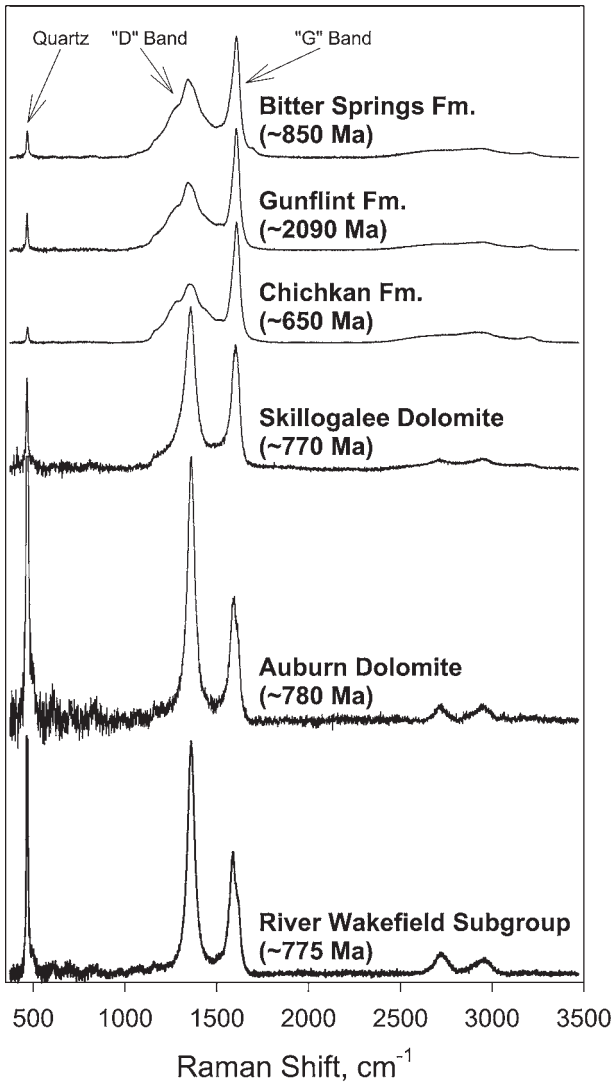

FIG. 7. Complete Raman point spectra (375–3,470 cm^{-1}) of kerogen comprising relatively well-preserved (Bitter Springs, Gunflint, Chichkan) and poorly preserved (Skillogalee, Auburn River Wakefield) fossils analyzed *in situ*, end-points of the continuum of geochemical maturation studied here (Figs. 1 and 9). With increasing maturation, the "D" band (at ~1,350 cm^{-1}) changes from being broad, of relatively low intensity and bumpy, to being narrow, prominent, and sharp; the "G" band (at ~1,600 cm^{-1}) changes from a single band centered at ~1,620 cm^{-1} to being bifurcated with the increasingly prominent component centered at ~1,580 cm^{-1}; and second-order Raman bands (at ~2,700 cm^{-1} and ~2,900 cm^{-1}) become increasingly evident. The band at ~480 cm^{-1} in all spectra is that of quartz, the crystalline matrix in which the permineralized fossils are embedded.

for 10 s, which resulted in a total data collection time of 100 min for each image. The several hundred spexels thus obtained for each specimen were then processed (using the Dilor operating PC program, LabSpec version 2.08) by constructing a map of the intensity in the spectral window corresponding either to the "D" band (at ~1,350 cm^{-1}) or the "G" band (~1,600 cm^{-1}) of the kerogenous material analyzed, with maps made by use of the "G" band being generally of relatively higher Raman image quality. The resulting two-dimensional "molecular–structural maps" show the spatial distribution in the analyzed fossils of the carbonaceous molecular structures that produced the spectral bands of their kerogenous constituents, with the varying intensities in such images corresponding to the relative concentrations of such structures detected (Figs. 2 and 4). Three-dimensional virtual Raman images have been prepared by "stacking" a digitized series of such two-dimensional maps (Schopf, 2003).

Deconvolution of spectra. The deconvolution procedure applied here to resolve spectra into their various components, each having a band shape that can be described by a mixture of Gaussian and Lorentzian mathematical functions, involves a series of curve-fitting techniques performed by use of PeakFit version 4.02 software (formerly, Jandel Scientific, San Rafael, CA). Three statistical criteria have been used to assess the results obtained: (1) the "goodness of fit," defined as r^2, the coefficient of determination, an index of the closeness of fit between the original spectrum and the totality of the fitted components; (2) the "stability of fit," a measure of the robustness of the fit with respect to changes in such parameters as the relative intensity, width, and spectral position of the fitted constituent bands; and (3) the parsimonious "best fit," an index of the match of the original spectrum to fitted curves composed of the smallest number of constituents.

Measures of preservation

Metamorphic grade. Listed in Table 1 are mineral-based metamorphic grades/facies reported for 17 of the 22 geologic units from which fossils are here analyzed. However, because most of these units occur over large geographic areas that have been affected variably by regional metamorphism, and because virtually no metamorphic data are available from the specific localities sampled, these reported grades/facies do not constitute precise indicators of the metamorphic history (and, thus, of the geochemical maturity) of the kerogenous materials analyzed. Moreover, many of the fossils and associated particulate kerogens

studied occur in terrains appreciably less altered than those to which mineralogically defined metamorphic categories can be applied—terrains in which minerals remain unchanged but organic components are significantly altered. Thus, such categories as "unmetamorphosed," "essentially unmetamorphosed," and "slightly to moderately metamorphosed" are too nondescript to provide more than a general basis by which to evaluate the degree of alteration of fossil organic material. Similarly, as estimated from the series of temperature–pressure regimes shown by Klein and Hurlbut (1985, pp. 499, 505), "subgreenschist" (<250°C), "lowest greenschist" (~250–300°C, 2–6 kb), "lower greenschist" (~250–350°C, 2–8 kb), and "greenschist" (~250–450°C, 2–10 kb) are too broad to be used in more than a general sense to indicate conditions responsible for the changes in the chemical–structural characteristics of the kerogens analyzed.

Nevertheless, as is shown in Table 1, it is notable that there is a strong correlation between the reported metamorphic grades/facies of the fossiliferous units sampled and all other measures of the quality of preservation of their contained organic-walled microscopic fossils (*viz*., fidelity of fossil preserveration, kerogen color, H/C and N/C ratios of bulk-sampled kerogens, and the RIP).

Fidelity of fossil preservation. The fidelity of preservation of fossils in each of the 22 units studied is listed (Tables 1 and 2 and Fig. 1) as belonging to one of four gradational categories: excellent, good, fair, and poor. This subjective evaluation (by J.W.S.) is based on the preservation of various biologic structures (cell walls, terminal cells, and encompassing sheaths) in fossils observed in the petrographic thin sections examined in the present study, not on the quality of preservation exhibited by fossils reported from the units in previous publications. Thus, for example, although some microorganisms exhibiting "good" preservation have been described from the Duck Creek Dolomite (Knoll and Barghoorn, 1976; Knoll *et al*., 1988), the preservation of fossils in the samples studied here is categorized as "poor." Further, although fairly well-preserved fossils are known from cherts of both the Paradise Creek (Licari *et al*., 1969) and McLeary (Hoffman, 1976) Formations, it should be noted that no fossils were detected in the samples used in this study collected from these units at the previously reported fossiliferous localities (Tables 1 and 2).

Kerogen color. Several techniques are used routinely by organic geochemists to estimate the maturity of fossil organic matter, most commonly measurements of hydrogen to carbon abundances (*e.g*., Strauss and Moore, 1992) or of microscopically determined vitrinite reflectance (*e.g*., Hunt, 1996; Vandenbroucke, 2003). However, H/C ratios (such as those listed in Tables 1 and 2) can be measured by current analytical techniques only on bulk samples of acid-macerated kerogens, not on individual microscopic fossils or kerogen particles. Further, measurements of vitrinite reflection depend on the presence of vitrinite, a major maceral only in Type III (higher plant-derived) kerogens (Vandenbroucke and Largeau, 2004), whereas the Precambrian kerogens studied here (permineralized in rock units that appreciably predate the origin of higher plants) are, by definition, Type I, derived from organic matter of microbial/algal origin. Such techniques, therefore, are of limited use in defining the geochemical maturity of kerogens that comprise the individual microscopic fossils analyzed here by Raman imagery. For such reasons (and because the instrumentation required for measurements of H/C ratios and vitrinite reflectance is not readily available to most paleobiologists), the color of preserved kerogen—ranging with increasing geochemical maturity from amber to amber brown to brown to black (Tables 1 and 2)—has come to be widely used in paleobiology as a rough index of the fidelity of organic geochemical preservation (Peters *et al*., 1977).

As is the standard paleobiologic practice in determination of kerogen color, an initial assessment of the color of the specimens studied here was made by optical microscopy and visual inspection of multiple photomicrographs taken under uniform conditions of each of the objects analyzed (Peters *et al*., 1977). To minimize the uncertainties of such assessment and to standardize color designations, we have used a five-stage procedure, introduced here, that allows quantitative comparison of kerogen color with other measures of its preservation: (1) Representative microfossils from each assemblage were located and photographed under uniform conditions; (2) a computerized color scanner was used to digitize the photomicrographic prints; (3) the resulting digital images were displayed in Adobe Photoshop

software and color-matched to the prints; (4) using this software, values for red, green, and blue (RGB) were recorded at 20 points in the image of each object (10 at relatively thick parts of each specimen, 10 in thinner regions); and (5) the resulting 20 values were averaged and converted to a percent value (by normalizing total intensity to 100%) to yield an RGB set for each specimen. Because the green component was found to be essentially constant (33.6 ± 1.7%) for the kerogens in the 22 geologic units thus analyzed, we have used here the ratio of the red to the blue component of such measurements, R/B, as the indicator of kerogen color. (In future studies, as use of digitized photomicrographic cameras becomes increasingly widespread in paleobiology, the second step in this sequence, the use of a computerized color scanner to digitize optical photomicrographic prints, can be eliminated.)

By use of this procedure, the well-established gradational color changes in kerogens of increasing maturity included in the range of alteration of those here studied (Gutjahr, 1966; Staplin, 1969; Peters *et al*., 1977) have been defined quantitatively, as listed in Table 2: R/B > 2.0 (amber brown); 2.0–1.5 (brown); 1.4–1.0 (dark brown); 0.9–0.5 (brownish-black); and <0.5 (black).

H/C and N/C ratios of bulk samples of kerogens. The ratios of hydrogen to carbon and of nitrogen to carbon listed in Table 1 and summarized in Table 2 are those reported by Strauss and Moore (1992, Tables 17.5 and 17.9), measured on bulk samples of kerogens isolated by acid maceration of the various fossil-bearing rock units by use of procedures summarized by Strauss *et al*. (1992a,b, and references therein).

PALEOBIOLOGIC APPLICATIONS AND LIMITATIONS OF LASER-RAMAN IMAGERY

Raman spectroscopy, of well-established use for analyses of the chemical–structural characteristics both of minerals (*e.g*., McMillan and Hofmeister, 1988; Williams *et al*., 1997) and of dehydrated carbonaceous matter freed from rocks by acid maceration (Pasteris and Wopenka, 1991, 2003; Jehlicka and Beny, 1992; Wopenka and Pasteris, 1993; Yui *et al*., 1996; Spotl *et al*., 1998; Kelemen and Fung, 2001; Jehlicka *et al*., 2003), can be used also, as is shown here, to analyze the kerogenous components of permineralized organic-walled fossils and associated sapropelic debris whether *in situ* or in aqueous acid-resistant residues, including those that have been dried and subsequently rehydrated. As is shown in the following section, such rehydration significantly enhances details of the acquired Raman spectra. In contrast with previous studies based on single-point Raman analyses of carbonaceous materials (cited above), the present study focuses on the use of Raman imagery: a technique that, by combining data obtained by measurement of large numbers of point spectra acquired from individual microscopic specimens, provides a means for direct high-resolution spatial correlation of optically discernible morphology and chemical–structural characteristics.

Applications

Of broad applicability in paleobiology, Raman spectroscopy can be used not only to determine the chemical–structural characteristics of cell walls and other anatomical components of megascopic fossil plants (Kudryavtsev *et al*., 2001), but also to analyze carbonaceous specimens fossilized by either of the two modes of preservation most common in Precambrian sediments (Schopf, 1992b)—compressed fossils preserved as flattened remnants in fine-grained clastic sediments and analyzed by measurement of point spectra acquired at exposed surfaces (Arouri *et al*., 2000; Kaufman and Xiao, 2003); and permineralized (petrified) fossils three-dimensionally preserved in chemically deposited units, such as cherts, and analyzed in petrographic thin sections, most effectively by Raman imagery (Fig. 4). Such imagery, applicable to studies of individual organically preserved microorganisms as small as ~1 μm in diameter, can be used to construct "molecular–structural maps" of individual fossils or of selected parts of such fossils, both in two (Fig. 4) and in three (Schopf, 2003) dimensions. Raman images can be acquired of specimens either in aqueous acid-resistant residues, freed from their encompassing matrix by palynological maceration (Fig. 2c), or in petrographic thin sections (Fig. 4). And in thin sections, images can be obtained whether the fossils are exposed at the surface of or embedded within the section studied, and whether the sections are polished or are unpolished and covered by a thin veneer of microscopy immersion oil (Fig. 4) (Schopf *et al*.,

2002a). Moreover, because Raman spectroscopy can be used to characterize minerals as well as fossilized organic matter, Raman imagery provides a means by which to: (1) identify the mineralic components of permineralized carbonaceous fossils, such as the fine-grained quartz in which the fossils studied here are three-dimensionally embedded (Fig. 7); (2) map the spatial relations between such minerals and preserved organic matter; and (3) identify the inorganic constituents of mineral-replaced microfossils, the third most common mode of preservation of Precambrian microbes (*e.g.*, Cloud and Licari, 1968; Gutstadt and Schopf, 1969; Walter *et al.*, 1976; Hofmann and Schopf, 1983; Hofmann and Grotzinger, 1988; Schopf, 1993). A technique that is both non-destructive and non-intrusive, Raman imagery can be applied even to specimens such as those archived in museum collections to protect them from physical or chemical alteration (Schopf *et al.*, 2002a).

Hydrated versus dehydrated isolated kerogens. Unlike the specimens on which this study is centered—fossils and particulate kerogens preserved by permineralization and analyzed *in situ* (Figs. 3 and 4) or in aqueous acid-resistant residues (*e.g.*, Fig. 2)—previous Raman studies of ancient carbonaceous matter have focused chiefly on particulate kerogens preserved by compression and analyzed in a dehydrated state, isolated by acid maceration from their encompassing matrices (Pasteris and Wopenka, 1991, 2003; Jehlicka and Beny, 1992; Wopenka and Pasteris, 1993; Yui *et al.*, 1996; Spotl *et al.*, 1998; Kelemen and Fung, 2001; Jehlicka *et al.*, 2003; Nestler *et al.*, 2003). Published spectra of such dehydrated carbonaceous matter are relatively simple, consisting of two more or less symmetric major bands (the "D" band, at ~1,350 cm^{-1}; and the "G" band, at ~1,600 cm^{-1}). However, results reported here acquired by analyses of dehydrated kerogens prepared by standard techniques (as dried powders or individual fossil specimens, and as particulate kerogens prepared by compaction, compression, or pelletization in KBr) show that for organic-walled fossils and particulate kerogens preserved by permineralization, such dehydration obscures significant spectral information. In particular, we carried out experiments on the sequential hydration–dehydration–rehydration of relatively well-preserved fossils and particulate kerogens isolated by acid maceration from five of the 22 fossil-bearing cherts studied (those of the Tremadocian of Poland and of the Chichkan, Min'yar, Bitter Springs, and Gunflint Formations; Tables 1 and 2). Results obtained, both from optical images acquired under the same conditions at each step of the sequence (*e.g.*, Fig. 2d) and from measurement of Raman spectra (*e.g.*, Figs. 2e and 8), can be summarized as follows:

1. Upon dehydration, the Raman spectra change markedly. The bumpy, evidently multicomponent, asymmetric "D" band exhibited by spectra of permineralized specimens analyzed *in situ* and by spectra of hydrated specimens analyzed in aqueous acid-resistant residues transforms into a more or less featureless symmetric band (Figs. 2e and 8); the "G" band appreciably broadens (*e.g.*, from 60 to 78 cm^{-1}; Fig. 2e); and the strength of the Raman signal decreases by a factor of 10–20, evidencing increased absorption by the dehydrated specimens of the excitation and backscattered laser light.
2. The optical properties of such fossils also change markedly upon dehydration, from being lighter colored/less intense in a hydrated condition (and having optical properties like those of fossils analyzed *in situ*) to being darker/more intense upon dehydration (Fig. 2d), a change that evidences the increased absorption by the dehydrated specimens of visible light.
3. Such spectral and optical changes are reversible (Fig. 2d and e) within seconds (upon rehydration) or several minutes (for specimens completely dehydrated), a reversibility exhibited by specimens repeatedly dried and rehydrated, and observed to occur even in specimens dried for 2.5 months (data not here shown).

Thus, although information-rich Raman spectra can be obtained from relatively well-preserved permineralized fossils and particulate kerogen analyzed *in situ* and in aqueous acid-resistant residues, appreciable chemical–structural information is masked in spectra acquired from such materials analyzed in dehydrated acid-resistant residues. Significant insights have been acquired by Raman studies of isolated dehydrated particulate kerogens preserved by compression (Pasteris and Wopenka, 1991, 2003; Jehlicka and Beny, 1992; Wopenka and Pasteris,

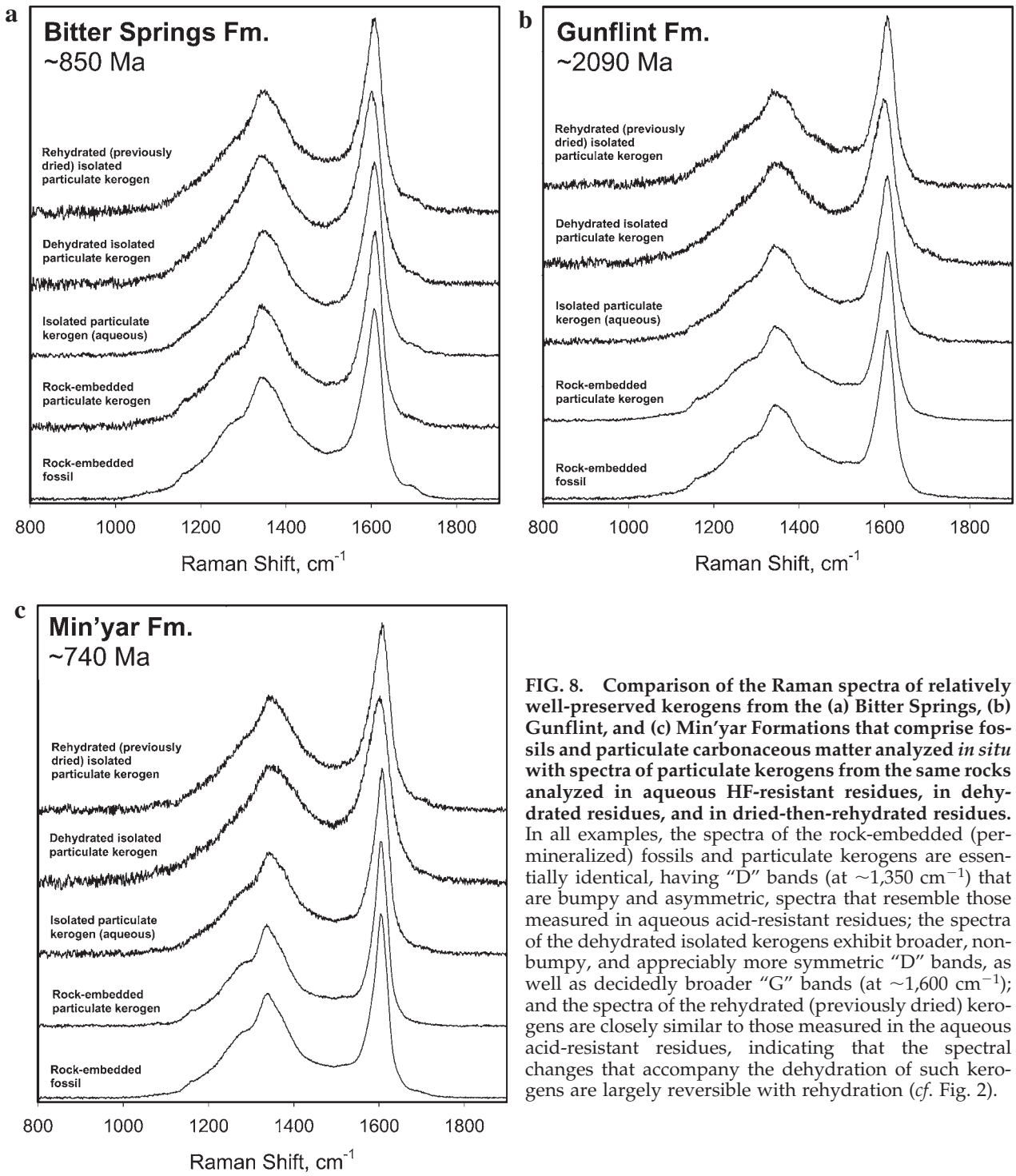

FIG. 8. Comparison of the Raman spectra of relatively well-preserved kerogens from the (a) Bitter Springs, (b) Gunflint, and (c) Min'yar Formations that comprise fossils and particulate carbonaceous matter analyzed *in situ* with spectra of particulate kerogens from the same rocks analyzed in aqueous HF-resistant residues, in dehydrated residues, and in dried-then-rehydrated residues. In all examples, the spectra of the rock-embedded (permineralized) fossils and particulate kerogens are essentially identical, having "D" bands (at ~1,350 cm^{-1}) that are bumpy and asymmetric, spectra that resemble those measured in aqueous acid-resistant residues; the spectra of the dehydrated isolated kerogens exhibit broader, nonbumpy, and appreciably more symmetric "D" bands, as well as decidedly broader "G" bands (at ~1,600 cm^{-1}); and the spectra of the rehydrated (previously dried) kerogens are closely similar to those measured in the aqueous acid-resistant residues, indicating that the spectral changes that accompany the dehydration of such kerogens are largely reversible with rehydration (*cf.* Fig. 2).

1993; Yui *et al.*, 1996; Spotl *et al.*, 1998; Kelemen and Fung, 2001; Jehlicka *et al.*, 2003; Nestler *et al.*, 2003), but for permineralized carbonaceous matter, such results have evidently provided only a part of the spectral information potentially measurable.

Limitations

Though useful for investigating a wide variety of paleobiological materials, Raman imagery is not without limitations. For example, point spectra can be acquired from the upper side of opaque

coaly fossils exposed on fractured rock surfaces (Arouri *et al*., 2000; Nestler *et al*., 2003) or from carbonaceous cellular remnants embedded in cellulose acetate peels (Walton, 1928; Joy *et al*., 1956) of calcitic coal balls (results not here shown). But Raman images of the underlying structures of such specimens can be obtained only if the fossils are, like those of permineralized fossil woods or microbial assemblages analyzed in petrographic thin sections, capable of transmitting light. Moreover, because in such relatively translucent sections with increasing depth the effects of spherical aberration result in decreased spatial resolution and, accordingly, a decrease in the backscattered signal acquired, distinct images are generally obtained from specimens situated near the upper surface of a thin section. Finally, because the Raman signal can be distorted by scattering at surficial interfaces, specimens analyzed in thin sections that have overlying coverslips generally yield images less distinct than those analyzed in uncovered sections.

In comparison with Raman spectra of minerals, those of the relatively well-preserved kerogens studied here (*e.g*., Figs. 2e and 8) are broad and complexly bumpy, a lineshape pattern that suggests they are composed of a combination of bands. Though interpretation of such lineshapes can be clarified by spectral deconvolution, this solution has limitations. In particular, deconvolution cannot be used to dissect the spectra of geochemically immature kerogens in which abundant hydrogen-saturated structures (mostly, small aromatic molecules) produce strong broad fluorescence. Interference by such fluorescence thus presents a significant problem in analyses of organic-walled fossils permineralized in especially little altered deposits—such as the unmetamorphosed, Eocene-age, Clarno chert (Kudryavtsev *et al*., 2001; Czaja *et al*., 2002)—or of specimens in acid-resistant residues mounted in fluorescence-producing organic media (a problem easily overcome by analyzing water-mounted preparations; Figs. 2e and 8). However, because all of the kerogens analyzed in the present study are relatively mature, composed chiefly of aggregates of fairly large PAHs (as documented below), and because the condensation of aromatics leading to the formation of such compounds shifts fluorescence to increasingly longer wavelengths (Lumb, 1978), the fluorescence of such materials in the red to near-infrared regions of the spectrum has not affected the Raman measurements made here by use of green or blue visible light.

Optimum results

Acquisition of high-resolution Raman images from permineralized fossils and associated carbonaceous matter analyzed *in situ* is principally affected by three factors: (1) the size of the objects analyzed, especially minute (submicron-sized) objects yielding relatively poor results; (2) the depth of the objects within the thin section studied, with increasing depth yielding decreasing resolution; and (3) the presence of nearby kerogenous detritus, which can have a signal-blurring effect on the image obtained. As shown here, parts of fossils as small as $\sim$1 μm in size can be imaged effectively (Fig. 4), with increased image quality obtainable by use of increasingly long image-acquisition times. Over typical total acquisition times of $\sim$100 min, Raman images can be acquired of fossils situated within the uppermost $\sim$30 μm of petrographic thin sections. Our best results have been acquired by analyses of fossils well separated from associated organic detritus and situated at or near the upper surface of microscopy immersion oil-veneered petrographic thin sections.

INTERPRETATION OF THE RAMAN SPECTRA

Prominent vibrational bands

The three most prominent features of the Raman spectra of the fossils analyzed here are (1) a group of bands centered at 1,300–1,350 cm^{-1} (Figs. 2e, 6a, and 7–10); (2) a band of high intensity at $\sim$1,600 cm^{-1} (Figs. 2e, 6a, and 7–10); and (3) a group of weaker bands in the $\sim$3,000 cm^{-1} region (Fig. 7). In notable respects, these spectra resemble those of graphitic and other geochemically less altered carbonaceous materials characterized by dominant "D" (disordered) and "G" (graphitic) bands at $\sim$1,350 cm^{-1} and $\sim$1,600 cm^{-1}, respectively, and a second-order band at $\sim$2,700 cm^{-1} (Tuinstra and Koenig, 1970) that seems generally comparable to the group of bands in the $\sim$3,000 cm^{-1} region present in spectra of the fossils. Such similarity, however, applies strongly only to the relatively poorly preserved fossils analyzed (Figs. 7 and 9, lower spectra), whereas the better-preserved specimens

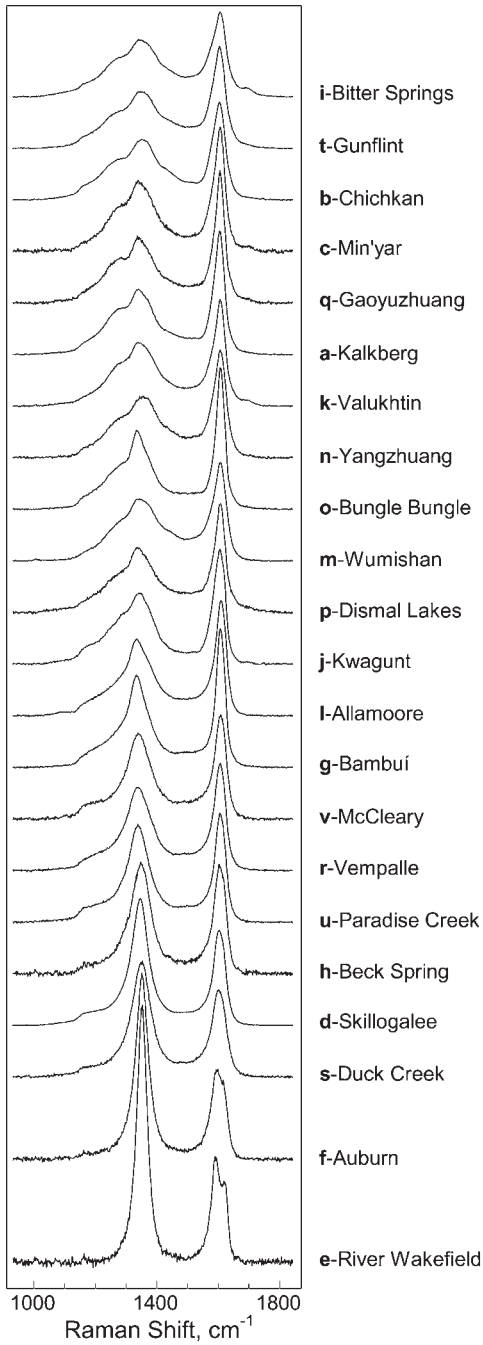

FIG. 9. Raman point spectra of kerogenous fossils (and for the Paradise Creek and McLeary Formations, of wispy clouds of kerogen) from the 22 cherts here analyzed, ordered from top to bottom by their decreasing RIP value (Table 2). With decreasing RIP values, the prominent vibrational "D" band at ~1,350 cm^{-1} becomes increasingly sharper, having fewer subsidiary bands and markedly less breadth; the other prominent vibrational ("G") band, at ~1,600 cm^{-1} and made up of two components, initially narrows and becomes increasingly peaked (**i–g,** the uppermost 14 spectra) and then gradually broadens and decreases in intensity (**v–e,** the lowermost eight spectra) as one of its constituents (at ~1,620 cm^{-1}) becomes less prominent and the other (at ~1,580 cm^{-1}) increases in intensity to bifurcate the band into its two component peaks (h–e, the lowermost five spectra).

(Figs. 7 and 9, upper spectra) have Raman signatures that distinctly differ from that of graphite (Fig. 6a, lowermost spectrum).

All three of the prominent spectral features of the fossils are characteristic of the Raman spectra of molecular subunits of interlinked aromatic hydrocarbons. Carefully studied and well-documented examples of such compounds include PAHs (Mapelli *et al*., 1999a,b; Rigolio *et al*., 2001; Castiglioni *et al*., 2001a,b; Negri *et al*., 2002); polyparaphenylene-based hydrocarbons (Marucci *et al*., 1999); and lignin and lignin-like molecules (Agrawal and Ralph, 1997). The shared structural feature of such materials is the presence of benzenoid six-membered aromatic rings, which, unlike the subunits of graphite, are relatively hydrogen rich. In such aromatics, the most intense Raman band, at ~1,600 cm^{-1}, is ascribed to synchronous aromatic ring-stretching vibration [the so-called "Я" motion of PAHs (Mapelli *et al*., 1999b)]; the bands within the 1,200–1,400 cm^{-1} range, to modes of aromatic ring deformation and totally symmetric breathing [the "Ⱥ" motion in PAHs (Mapelli *et al*., 1999b)]; and the bands in the ~3,000 cm^{-1} region, to either the second-order spectrum of such aromatics or to aromatic and aliphatic C-H stretching. However, in agreement with results of theoretical modeling (Negri *et al*., 2002), bands due to symmetric C-H vibrations at ~3,000 cm^{-1}, present in the spectra of many organic compounds (Tu, 1982; Lin-Vien *et al*., 1991), are weak and virtually undetectable in relatively large PAHs (Mapelli *et al*., 1999a). Hence, although elemental analyses of the fossil kerogens show them to contain atomic hydrogen (Tables 1 and 2) that, on the basis of the broad, bumpy, evidently multicomponent "D" bands in spectra of the better-preserved fossils, can be inferred to be bound to PAHs (Castiglioni *et al*., 2001a,b), definitive evidence of such bonding cannot be expected to be provided by Raman analysis.

Thus, the Raman spectra of the fossils studied are consistent with a large body of data, establishing that kerogens are composed predominantly of more or less regularly stacked arrays of interlinked PAHs (Durand, 1980). In particular, we interpret the Raman data to indicate that the relatively poorly preserved, geochemically more altered fossils (Figs. 7 and 9, lower spectra) are composed of kerogens having a relatively ordered overall structure made up chiefly of fairly large and therefore hydrogen-poor PAHs, whereas the kerogens that comprise the less altered specimens (Figs. 7 and 9, upper spectra) are composed of

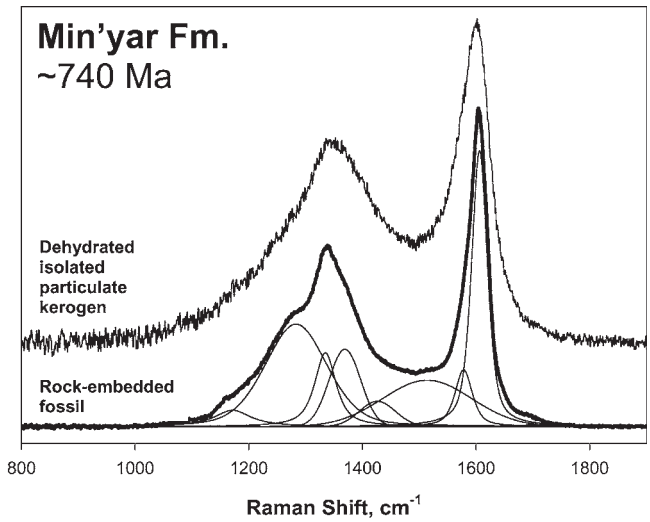

FIG. 10. Raman spectrum of an unnamed cylindrical filament from the Min'yar Formation (Figs. 3c and 4c) analyzed *in situ* (middle broad-lined spectrum), compared with that of dehydrated particulate kerogen isolated from the same rock (uppermost spectrum) and results of deconvolution of the spectrum acquired *in situ* (lowermost thin-lined spectra) showing it to be composed of nine subsidiary bands having a goodness of fit of 0.999643.

more irregularly stacked arrays of PAHs that are smaller and comparatively hydrogen rich. This interpretation is in agreement with results of detailed studies of kerogen maturation (Vandenbroucke, 2003; Vandenbroucke and Largeau, 2004), including those based on electron paramagnetic resonance analyses (Durand *et al*., 1977), dark-field imaging and diffractometry by transmission electron microscopy (Oberlin *et al*., 1980), ring condensation index calculations (van Krevelen, 1993, p. 357), and three-dimensional molecular modeling (Faulon *et al*., 1989; Vandenbroucke and Largeau, 2004).

Other spectral features

Unlike the other features of the Raman spectra of the kerogens studied here, two bands stand out as not being evidently relatable to aromatic hydrocarbons. One of these, at ~1,170 cm^{-1} (Figs. 6a and 7–10), is relatively heat stable, detectable in the spectra of well-preserved fossils experimentally heated to 800°C, a temperature at which such spectra typically exhibit additionally only a "G" band and a symmetric "D" band (Fig. 6a). Although this band is similar in position to a weak quartz band (at ~1,159 cm^{-1}), spectral data rule out the matrix chert as its source: (1) Because of its low intensity (in pure quartz, about 5% that of the major quartz band at ~467 cm^{-1}), the contribution of the quartz band at ~1,159 cm^{-1} to the spectra of the relatively well-preserved chert-embedded fossils studied here is demonstrably negligible (Fig. 7); (2) this weak quartz band, having a breadth of ~10 cm^{-1} (full width at half maximum), is appreciably narrower than the >40 cm^{-1}-broad heat-stable band at ~1,170 cm^{-1} present in the spectra of such fossils (Fig. 7); and (3) unlike the quartz band at ~1,159 cm^{-1}, the band at ~1,170 cm^{-1} is present in spectra of organic materials completely devoid of silica, such as plant fossils permineralized in calcitic coal balls (results not here shown) and heat-treated paraformaldehyde (Gogotsi and Nickel, 1998).

Thus, we assign the relatively heat-stable band at ~1,170 cm^{-1} to the symmetric stretch of carbon to carbon single bonds of C—C═C—C bridges that link aromatic domains—for example, of linear polyenes, $(—CH═CH)_n$, $n < 10$ (Schafer *et al*., 1991); of two-bridged benzene rings, *e.g*., *trans*-1,2-diphenylethylene [SDBS (Integrated Spectral Data Base System for Organic Compounds)#1844(http://www.aist.go.jp/RIODB/SDBS/menu-e.html); see also Aldrich Data Base CAS #103-30-0 (http://www.sigmaaldrich.com)]; and of three-bridged benzene rings, *e.g*., 1,4-bis(2-methylstyryl)benzene [Sigma-Aldrich Data Base CAS #13280-61-0 (http://www.sigmaaldrich.com)].

In contrast with this heat-stable component, the other non-aromatic spectral feature—at ~1,697 cm^{-1} (Figs. 7, uppermost spectrum; 8a and c, lowermost spectra; and 9i, c, q, and k)—disappears upon heat treatment to temperatures of ~500°C (Fig. 6a). Observed only in the spectra of especially well-preserved fossils (having RIP values, as defined below, of >8.4; Table 2), we interpret this heat-labile band to reflect the symmetric stretch vibration of C═O carbonyl groups. Associated with the aromatic hydrocarbons of kerogens, such oxygen-containing moieties—for example, in aliphatic esters, aldehydes, and ethers—have been pro-

posed as bridging links between kerogenous aromatic domains (Forsman, 1963; Siskin and Katritzky, 1991).

"Kerogen signal"

Characteristics of the signal of well-preserved kerogens. Three lines of evidence, illustrated by spectra acquired from the relatively well-preserved carbonaceous matter analyzed here (Fig. 9i–r, the uppermost 16 spectra), comprise what we consider to constititute the signature of well-preserved "kerogen" (cf. Kudryavtsev *et al*., 2001)—fossilized organic matter of assured biological origin—rather than of graphite, of possibly nonbiologic origin:

1. Presence of a shoulder on the low-frequency side of the "D" band. In the spectra of such well-preserved specimens, the "D" band is asymmetric and composed of subsidiary components of which one, a strong peak centered at ~1,270 cm^{-1}, corresponds to a prominent shoulder on the low-frequency side of the "D" band. In contrast, in spectra of less well-preserved, more graphitized fossils (Fig. 9u–e, the lowermost six spectra) and of crystalline graphite (Fig. 6a, lowermost spectrum), the "D" band (if present) is more symmetrical, a single band devoid of subsidiary components (Matthews *et al*., 1999). Like the spectra of the well-preserved fossils, those of PAHs commonly exhibit two or more Raman bands in the ~1,300 cm^{-1} region (Castiglioni *et al*., 2001a).
2. Lack of shift of the "D" band center with laser excitation wavelength. In disordered graphite, the position of the "D" band varies with excitation laser photon energy (~50 cm^{-1}/eV) via a resonance Raman process (Vidano *et al*., 1981; Matthews *et al*., 1999). No such energy-dependent shift was observed in the Raman spectra of any of the relatively well-preserved specimens analyzed at five excitation laser wavelengths that ranged from the blue (2.61 eV) to the infrared (1.65 eV) (at a detection limit of ~10 cm^{-1}/eV).
3. Absence of a graphite-characteristic second-order band. Virtually all non-fossil graphitic materials exhibit a prominent well-defined second-order band at ~2,700 cm^{-1} (Vidano *et al*., 1981), a wavelength frequency about twice that of the "D" band, which was not observed in the spectra of any of the relatively well-preserved specimens analyzed here (*e.g*., Fig. 7, uppermost three spectra). This second-order band is sensitive to the regularity of stacking of graphene layers, the three-dimensional ordering of the planar subunits of graphite and graphite-like materials (Lespade *et al*., 1982). As in the spectra of the relatively well-preserved fossils, this band is absent even from the spectra of large flat PAH molecules, the two-dimensional structure of which rather closely resembles that of the subunits of graphite.

Taken together, we regard these three indicators to constitute a distinctive "kerogen signal" characteristic of geochemically altered, relatively immature to moderately mature biogenic organic matter, a signal easily discernible in the better-preserved fossils here studied (Fig. 9i–r, the uppermost 16 spectra) that becomes progressively less evident in increasingly more graphitized specimens (Fig. 9u–e, the lowermost six spectra).

Changes in the "kerogen signal" with dehydration. Unlike the narrow sharp bands typical of the Raman spectra of minerals (*e.g*., McMillan and Hofmeister, 1988; Williams *et al*., 1997)—such as crystalline graphite (Fig. 6a, lowermost spectrum) or the fine-grained quartz in which the fossils studied here are three-dimensionally embedded (Fig. 7)—Raman bands of all of the relatively well-preserved kerogens here studied, whether analyzed *in situ* or as isolated particles in water-mounted preparations, are notably broad, rounded, and evidently multicomponent (Figs. 2e, 6a, and 7–10). We interpret this complex pattern, evident particularly in the region centered at ~1,350 cm^{-1} (Figs. 7, uppermost three spectra; and 9i–r, the uppermost 16 spectra), to reflect the presence of closely spaced or overlapping subsidiary Raman bands. It is notable, however, that upon dehydration of particulate kerogens freed from the cherts by acid maceration, this pattern becomes obscured (Figs. 2e and 8).

Though deconvolution can help identify the components of such complex spectra (Fig. 10), it is important to note that numerous sets of differing subsidiary bands can yield curves that appear to fit the spectra measured. To avoid ambiguous results, the deconvoluted spectra have therefore been analyzed by use of multiple statistical tests (see Materials and Methods), and the results ob-

tained have been compared both with those acquired from analyses of scores of fossils from a single geologic unit (Fig. 11) and with those from the experimental heating of rock-embedded fossils carried out under controlled laboratory conditions (Fig. 6). This deconvolution procedure has been applied to the spectra of virtually all specimens studied here. One such example is shown in Fig. 10, the deconvoluted spectrum of a fossil filament from the metamorphically little altered Min'yar Formation (cf. Figs. 3c and 4c). Composed of nine subsidiary bands, this spectrum has a "goodness of fit" greater than 0.999. Fossils analyzed from more altered terrains (Table 1 and Figs. 7 and 9, lower spectra) typically have much simpler Raman spectra that more closely resemble those of graphite and graphite-like materials that can be fit by a curve made up of only three subsidiary bands (results not here shown).

Table 3 summarizes results of the deconvolution of spectra of kerogens comprising well-preserved fossils, analyzed *in situ*, from four of the cherts studied, together with those of spectra of particulate kerogens isolated from the same units and analyzed as dehydrated powders. Upon such dehydration, the "D" bands (~1,350 cm^{-1}) become markedly more symmetric because of the broadening (by an average of ~30%; Table 3) of their subsidiary components (cf. Figs. 2e and 8). Such broadening, generally ascribed to the onset of structural disorder (*e.g.*, Gilson and Hendra, 1970), is paralleled by a change in the optical properties of the kerogens, from being lighter colored/less intense in chert-embedded or isolated hydrated samples to becoming darker/more intense in dried samples (*cf.* Fig. 2d). The high optical absorption of such structurally disordered dried kerogens is well understood; absorption of visible light by graphite-like carbonaceous materials is attributable to weak π-bonding between graphene-like stacked sheets of hexagonally arrayed carbon atoms (Ubbelohde and Lewis, 1960)—such as those of the PAHs that are the major components of kerogens (Oberlin *et al.*, 1980; Vandenbroucke, 2003). Thus, the high absorption (and resulting black color) of the isolated dehydrated particulate kerogens results from the interaction of visible light and π-bonds that associate adjacent layers of such platy PAHs.

What mechanism could be responsible for the change upon dehydration of such kerogens from being structually more ordered to less ordered, lighter colored to darker? In answer, we note that the broad, evidently multicomponent, complex "D" band pattern that comprises the kerogen signal is exhibited only by relatively well-preserved specimens analyzed either *in situ*—in chert (Figs. 6a and 7–10) or in calcite (plant fossils analyzed in peels of Carboniferous coal balls, results not here shown)—or in aqueous acid-resistant residues (Figs. 2e and 8). All of these media are oxygen-rich (chert, SiO_2; calcite, $CaCO_3$; water, H_2O). From this, we suggest that the structure of the geomolecules of such kerogens—both *in situ* and in aqueous residues—may be stabilized by hydrogen bonding between the oxygen of the surrounding media and the peripheral hydrogens of the kerogenous PAHs. Such stabilization of parallel aligned platy kerogen subunits (Oberlin *et al.*, 1980) may account for the nanometer-scale stacked platelet substructure of the cell walls of permineralized microfossils analyzed *in situ* by

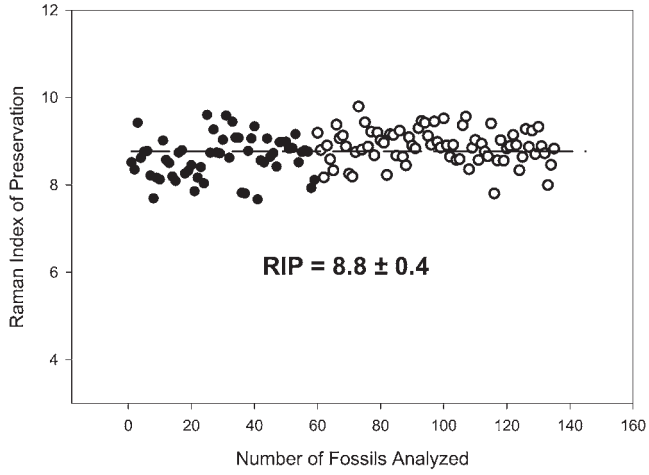

FIG. 11. RIP values and the mean value (denoted by the dashed line) for kerogens comprising 135 microfossils from the ~650–Ma-old Chichkan Formation of southern Kazakhstan showing that the SD (±0.4) of RIP values from the mean value (8.8) for the 135 fossils is ~4.5%. The close similarity of measurements obtained using a laser excitation wavelength of 531 nm, in the green portion of the spectrum (filled symbols; $n = 59$; RIP = 8.6, SD ±0.5), and those using 476 nm, in the blue portion (open symbols; $n = 76$; RIP = 8.9, SD ±0.4), shows that there is no significant difference between results acquired in these Raman studies by use of green or blue laser excitation.

Table 3. Measurements (Full Width at Half-Maximum) in Deconvoluted Spectra of the Prominent Raman Bands of Permineralized Kerogenous Fossils Analyzed *in Situ* Compared with the Broadening of These Bands that Accompanies Dehydration of Kerogens Isolated from the Same Geologic Units

	"D" band change						*"G" band change*			
Geologic unit (age), kerogen analyzed	*~1,280 cm^{-1}*	*%*	*~1,340 cm^{-1}*	*%*	*~1,375 cm^{-1}*	*%*	*~1,590 cm^{-1}*	*%*	*~1,610 cm^{-1}*	*%*
Chichkan Formation (~650 Ma)										
In situ fossil	139	22%	40	62%	52	19%	51	14%	38	5%
Isolated/dehydrated	169		65		62		58		40	
Min'yar Formation (~740 Ma)										
In situ fossil	129	16%	45	67%	65	40%	36	69%	33	49%
Isolated/dehydrated	149		75		91		61		49	
Bitter Springs Formation (~850 Ma)										
In situ fossil	125	6%	52	44%	57	47%	47	30%	38	18%
Isolated/dehydrated	133		75		84		61		45	
Gunflint Formation (~2,090 Ma)										
In situ fossil	152	2%	50	52%	57	26%	51	12%	37	32%
Isolated/dehydrated	155		76		72		57		49	
Average		12%		56%		33%		31%		26%

atomic force microscopy (Kempe *et al*., 2002). Thus, the obscuration of the spectral information that in specimens preserved by permineralization accompanies dehydration, as well as the onset in such materials of structural disorder and of changes in optical properties, may be due to molecular rearrangement that results in the closer packing of kerogenous PAHs and a replacement of H-bonds by π-bonds.

Though further studies will be needed to show whether this explanation is correct, there can be no doubt that for permineralized well-preserved kerogens isolated by acid maceration, an appreciable loss of spectral information accompanies dehydration (Figs. 2e and 8). In light of these findings, we suggest that reassessment may be required of results reported from previous Raman studies of such permineralized particulate kerogens analyzed in a dehydrated condition.

Changes in the "kerogen signal" with experimental heating. As an aid to identification of the subsidiary bands of the various Raman spectra acquired, we conducted a series of heating experiments on rock slices containing particularly well-preserved fossils designed to simulate the alteration of organic matter that accompanies low-grade metamorphism (see Materials and Methods). Results from such experiments, for one example presented in Fig. 6, can be summarized as follows:

1. <500°C. Only minor changes occur, chiefly a blurring of the multicomponent structure of the "D" band, due to the gradual broadening of its subsidiary components (changes similar to those observed upon kerogen dehydration; Figs. 2e and 8), and a decrease in "D" band peak intensity. Such changes, reflecting a progressive increase of structural disorder, may be due to the heat-induced breakage of H-bonds between rock-embedded polycyclic aromatics and the encompassing silica matrix
2. 500–900°C. The "D" band becomes increasingly symmetrical; its peak height (relative to the "G" band) increases; and the intensity of the subsidiary band at ~1,170 cm^{-1} gradually declines such that at 900°C it is essentially undetectable (Fig. 6a). These changes may reflect the increasing enlargement of PAHs and an accompanying loss of peripheral hydrogens, an interpretation that is in agreement with results of modeling of the conversion of PAHs to graphite (Negri *et al*., 2002).
3. >900°C. Unlike changes up to this temperature (referred to as "carbonization" by Fitzer *et al*., 1971), alterations above 900°C are uniformly regarded as "graphitization" (Ubbelohde and Lewis, 1960; Fischbach, 1971). Here, the relative intensity of the "D" band initially continues to rise (*e.g*., Matthews *et al*., 1996; Endo *et al*., 1998); then, at temperatures above 1,200°C, when dehydrogenation of the kerogenous PAHs is largely completed, "D" band intensity dramat-

ically decreases with the growth of large, highly ordered, graphite crystallites (*e.g.*, Nemanich and Solin, 1979).

The processes of graphitization mimicked in these heating experiments, a gradual growth and increase in the ordering of graphene subunits, have been documented by the Raman-based studies of Landis (1971), Nemanich and Solin (1979), Lespade *et al*. (1982), and Knight and White (1989), and involve an increase in both two-dimensional (within graphene layer) and three-dimensional (the stacking of such layers) regularity. In spectra presented in these earlier studies, such graphitization is reflected by a narrowing of the Raman bands and, ultimately, by subdivision of the "G" band into its two components, a doublet made up of bands at ~1,580 and ~1,620 cm^{-1} [changes well shown in spectra of the fossils analyzed here (Fig. 9u–e, the lowermost six spectra)]. With continued graphitization, such studies have shown that the 1,620 cm^{-1} band (like the "D" band, evidencing in-plane disorder) decreases and together with the "D" band eventually vanishes, while the band at 1,580 cm^{-1} (evidencing in-plane order) becomes more narrow and increasingly prominent as the kerogen is progressively altered toward a graphite end-product (Vidano *et al*., 1981; Matthews *et al*., 1999).

RIP

From the data presented above, it is evident that changes in the "D" band and of its prominent shoulder (centered at ~1,270 cm^{-1}) are sensitive indicators of the low-temperature alteration of the kerogens studied here. Thus, in order to compare quantitatively the numerous and varied Raman spectra acquired from the fossils studied here (Fig. 9), we have used the "D" band shoulder and its relationship to the entire "D" band of each spectrum as a prime index of the Raman-evidenced degree of the low-temperature alteration of the materials analyzed. This can be expressed by the parameter α, defined as follows:

$$\alpha = \frac{\int_{1,100}^{1,300} I(\upsilon)d\upsilon}{\int_{1,100}^{1,500} I(\upsilon)d\upsilon}$$

where $I(\nu)$ is a measure of the intensity, I, at the Raman shift, ν, as determined from a Raman spectrum. Parameter α thus provides an estimate of the relative intensity of the shoulder at ~1,270 cm^{-1} as a ratio of the areas under the spectral curves in the 1,100–1,300 cm^{-1} region (to reflect the major contribution of the "D" band shoulder at ~1,270 cm^{-1}) and the 1,100–1,500 cm^{-1} region (to include the contribution of the entire "D" band spectrum).

Among the kerogens studied here, major changes in the spectra of the "D" band of relatively well-preserved specimens (in particular, symmetrization of the band and the accompanying disappearance of its prominent ~1,270 cm^{-1} shoulder)—reflected by a decrease in the value of the α parameter—were exhibited mainly during early stages of alteration, as is shown both by the spectra in Fig. 9 and by results of heating experiments in which such changes were observed to be completed at temperatures of 550–600°C (Fig. 6a).

In all specimens analyzed, including those that were experimentally heated (Fig. 6), subsequent alteration was observed to mainly involve a progressive increase of graphitization. To take into account such later-stage changes, we have therefore used for this quantitative comparison of the acquired Raman spectra a second parameter, γ, which provides an estimate of the contribution of chemical–structural changes occurring at higher-temperature, graphitization-evidencing alterations of the "D" band peak at ~1,350 cm^{-1} expressed relative to the entire "D" band spectrum in much the same way as the α parameter relates its components to the total "D" band spectrum. Thus, the parameter γ is defined as:

$$\gamma = \frac{\int_{1,300}^{1,370} I(\upsilon)d\upsilon}{\int_{1,100}^{1,500} I(\upsilon)d\upsilon}$$

The γ parameter, therefore, is a ratio of the areas under the spectral curves in the 1,300–1,370 cm^{-1} region (to reflect the major contribution of graphitization-evidencing changes in the "D" band at ~1,350 cm^{-1}) and the 1,100–1,500 cm^{-1} region (to include the contribution of the entire "D" band spectrum).

As thus defined, the two parameters, α and γ, are mathematically analogous. For both, selection of their relevant spectral windows is based on the

typical characteristics (band width and position) of their prominent components (for α, the "D" band shoulder; for γ, the graphitization-evidencing "D" band peak). In the kerogens studied here, the α parameter, a major component of the spectra of well- to moderately preserved fossils (Fig. 9i–r, the uppermost 16 spectra), decreases mainly during the early stages of geochemical alteration, whereas the γ parameter increases during the later stages of alteration as the kerogens become increasingly more graphitized (Fig. 9u–e, the lowermost six spectra).

On the bases of these analyses of both early- and late-stage changes in the Raman spectra of the geochemically relatively little altered kerogens here studied, we have devised a numerical parameter—for which we have coined the name RIP—intended to estimate quantitatively the fidelity of preservation (the extent of geochemical alteration) of naturally occurring kerogenous materials as evidenced by their Raman signatures. In formal mathematics, the RIP is defined as follows:

$$RIP = \frac{\alpha}{\gamma} = \frac{\int_{1,100}^{1,300} I(\upsilon)d\upsilon}{\int_{1,300}^{1,370} I(\upsilon)d\upsilon}$$

As a result, an RIP value represents the ratio of the areas under the spectral curves in the 1,100–1,300 cm^{-1} region (to reflect the major contribution of the "D" band shoulder at ~1,270 cm^{-1}) and the 1,300–1,370 cm^{-1} region (to reflect the major contribution of the graphitization-evidencing "D" band at ~1,350 cm^{-1}).

Such RIP values can be calculated directly from Raman spectra by use of any of various spectroscopic personal computer programs (such as LabSpec or PeakFit). In the present study, we have calibrated the RIP values of the 22 kerogens analyzed on a scale that ranges from a value of 1.0 (representing the most altered kerogen measured) to 9.0 (the "best-preserved," least altered kerogen). Carbonaceous matter more altered than that in the specimens studied here can be expected to have RIP values lower than 1.0. For example, graphitic particles analyzed in thin sections of amphibolite facies metasediments of the ~3,800-Ma-old Isua Supracrustal Group of southwestern Greenland have an RIP value of 0.6 (Fig. 6b). Similarly, kerogens less altered than the Precambrian samples analyzed here should have RIP values higher than 9.0. For example, cortical rootlets of the Carboniferous-age (~300-Ma-old) tree fern *Psaronius* permineralized in calcitic coal balls from Illinois that have an RIP value of 10.6 (data not here shown). Spectral changes (Fig. 6a) and changes in the RIP values (Fig. 6b) resulting from the experimental heating of individual fossils closely parallel those shown by the total suite of kerogens analyzed here (Fig. 9).

To obtain accurate RIP values, the spectra should first be normalized to the spectrographic response function, and the fluorescent baseline (if any) should be subtracted. Of course, RIP values so determined (and, thus, the ordering of the spectra shown in Fig. 9) are subject to uncertainty due to minor variations among the preserved kerogens in each of the geologic units—evidently, a maximum standard deviation (SD) of <5% (as discussed below), which indicates that any two kerogens having RIP values that fall within this range should be regarded as exhibiting essentially the same extent of geochemical alteration.

The RIP values calculated from the Raman spectra of kerogens measured in the 22 geologic units studied are listed in Tables 1 and 2. In Fig. 9, the spectra on which these RIP values were determined are ordered from top to bottom by decreasing RIP values, a measure of increasing geochemical maturity.

Variability of RIP values within a single geologic unit. Before applying the RIP concept to kerogens from the 22 geologic units studied, we analyzed the intra-geologic unit variation of RIP values by determining the SD from the mean of values measured from the spectra of numerous permineralized fossils in a relatively little altered representative unit, the Chichkan Formation of southern Kazakhstan, for which such deviation from the mean RIP value of 8.8 for 135 fossil specimens was ±0.4, a variation of ~4.5% (Fig. 11). The range of lineshapes of the Raman spectra acquired varied from fairly peaked and asymmetric (*cf*. Fig. 9, spectra q and o) to less peaked and more symmetrical (*cf*. Fig. 9, spectra t and b). Among the scores of Chichkan specimens thus compared were 107 spheroidal unicellular fossils (acritarchs and single-celled micro-algae) and 28 filamentous specimens, the preserved sheaths of *Lyngbya*-like oscillatoriacean cyanobacteria (*cf*. Fig. 3b). The mean RIP values of these morphological groupings was closely similar to that of the total population, and the deviation from the

mean within each grouping was <5%. Evidently, for kerogens altered to the extent of those measured here, there is little variability either among the RIP values measured for fossils from a single locality or of values measured on morphologically differing members of a single fossil community.

Comparison of RIP with previously proposed measures of geochemical maturity. Numerous studies have previously proposed use of the Raman signature of preserved carbonaceous matter as an index of geological metamorphic alteration (Jehlicka and Beny, 1992; Roberts *et al*., 1995; Yui *et al*., 1996; Spotl *et al*., 1998; Beyssac *et al*., 2002, 2003; Nestler *et al*., 2003). Unlike the present work, however, these earlier investigations—almost all focused on problems of metamorphic geology rather than paleobiology—center on graphitized, structurally highly altered materials preserved by compression, the uniformly simple spectra of which lack the complexity of those of the permineralized, relatively much less altered kerogens studied here. Indeed, as noted above, deconvolution of spectra of the relatively well-preserved fossils analyzed in the present study show them to be composed of at least nine subsidiary bands (Fig. 10), whereas those of the more graphitzed specimens can be fit by a curve made up of only three or fewer such bands. The previously suggested indices of organic maturation (Jehlicka and Beny, 1992; Roberts *et al*., 1995; Yui *et al*., 1996; Spotl *et al*., 1998; Beyssac *et al*., 2002, 2003; Nestler *et al*., 2003), most of which require mathematical manipulation of the spectra acquired, cannot be readily applied to geochemically relatively little altered kerogens such as those studied here because of their different spectral lineshapes.

In contrast, the RIP concept takes into account the complexity of the Raman spectra of submetamorphosed to little metamorphosed kerogens and is designed to be a simple tool based on direct measurement of Raman spectra that can be applied to carbonaceous matter encompassing all phases of organic geochemical alteration (from carbonization—diagenesis, catagenesis, and metagenesis—through graphitization and the ultimate formation of graphite). Though in need of further refinement (*e.g*., perhaps by use of the second derivative of the measured spectra), the RIP concept is a much needed attempt to tie together the totality of organic geochemical maturation in terrains ranging from submetamorphic to highly metamorphosed.

Summary

Raman spectra of the kerogens analyzed here establishes that they are composed predominantly of variably disordered and evidently interlinked arrays of moderately to extremely hydrogen-poor PAHs. Comparison of these spectra by use of the RIP, an approximate measure of the relative degree of geochemical maturity of such ancient carbonaceous matter, documents a progressive series of spectral changes that accompany the processes of incipient graphitization in unmetamorphosed and geologically little altered (lower greenschist facies and below) metamorphic terrains.

RESULTS AND SIGNIFICANCE

As is shown here, Raman imagery is a powerful technique that provides insight into the molecular–structural characteristics of carbonaceous matter permineralized in submetamorphosed and little metamorphosed ancient terrains. Because the kerogenous components of such deposits undergo a sequential series of changes as they become geochemically altered toward increasingly graphitized end-products—and because such changes can be quantified by use of the RIP, introduced here (Figs. 6b and 9)—such analyses provide effective means to measure the geochemical maturity of non-graphitic and incompletely graphitized ancient organic matter. Applied to individual organic-walled fossils, whether in acid-resistant macerations (Fig. 2) or in petrographic thin sections (Fig. 4), Raman imagery can be used also to demonstrate a one-to-one spatial correlation between optically discernible cellular morphology and carbonaceous (kerogenous) composition. Such correlation provides a strong new line of evidence by which to help evaluate the biogenicity of fossil-like objects of putative, but uncertain, biological origin, an important long-standing problem in Precambrian paleobiology (Awramik *et al*., 1983, 1988; Hofmann and Schopf, 1983; Schopf and Walter, 1983; Buick, 1984, 1988; Mendelson and Schopf, 1992; Brasier *et al*., 2002, 2004; van Zuilen *et al*., 2002; Cady *et al*., 2003; Schopf, 2004). These two particularly significant applications of Raman imagery—determination of the geochemical maturity of ancient kerogens and assessment of the biogenicity of ancient putative fossils—are addressed, in turn, below.

Geochemical maturity of permineralized kerogens

We have here used laser-Raman imagery to analyze *in situ* the molecular–structural characteristics of carbonaceous microscopic fossils and particulate kerogens preserved by permineralization in 22 fine-grained chert units ranging in age from Devonian to Paleoproterozoic. The Raman spectra acquired (Fig. 9) vary systematically with both the metamorphic grade of the fossil-bearing rock units sampled and the fidelity of optically discernible morphological preservation of the fossils studied (Tables 1 and 2), as well as with three other indices of the geochemical maturity of the kerogens of which the fossils are composed—their optically quantifiable color, and both the H/C and N/C ratios of particulate kerogens isolated by acid maceration from bulk samples of the fossil-bearing cherts. Shown in Fig. 12 are diagrams illustrating the relationships among several of these factors, the variations in each of which are strongly correlated with the geochemical maturity of the kerogens analyzed. Figure 12a and b document, respectively, the correlation of the H/C and N/C ratios with the color of the kerogens studied; Fig. 12c shows that the trend among the interrelated H/C and N/C ratios of the isolated kerogens correlates well with the fidelity of preservation of the morphologies of the fossils analyzed. Also illustrated are correlations between the RIP of the various kerogens and their optically measured colors (Fig. 12d) and both the H/C (Fig. 12e) and N/C (Fig. 12f) ratios of kerogens isolated from the same units.

All indicators of geochemical maturity considered here [including host-rock metamorphic grade and the fidelity of preservation of fossil morphology (not illustrated in Fig. 12)] vary systematically with the degree of alteration of the kerogens analyzed. Of particular note for paleobiologists is the consistent correlation among the various kerogens between changes in kerogen color and those of H/C ratios (Fig. 12a), N/C ratios (Fig. 12b), and RIP values (Fig. 12d). The color of preserved kerogen, whether comprising microscopic fossils (Gutjahr, 1966; Staplin, 1969) or present in the form of carbonaceous sapropelic particles (Peters *et al*., 1977), has long been used both in paleobiology, as an indicator of fidelity of preservation, and in the petroleum industry (Tissot and Welte, 1978; Hunt, 1996), as an index of source rock potential. That such color changes correlate not only with the H/C and N/C ratios, geochemically well-established measures of kerogen maturity (Peters *et al*., 1977; Tissot and Welte, 1978; Hunt, 1996), but also with the RIP values augurs well for the validity of this first use of the RIP to estimate quantitatively the degree of maturation of kerogenous materials occurring in submetamorphosed and little metamorphosed (lower greenschist facies) geologic units. Moreover, at relatively low RIP values, the "G" (~1,600 cm^{-1}) band becomes subdivided into a doublet, a feature reflecting incipient graphitization that is well illustrated by spectra of most altered kerogenous fossils studied here (Figs. 7, lower spectra, and 9u–e, the lowermost six spectra). Such spectra are closely similar to those of the least metamorphically altered (structurally most disordered) graphitic materials analyzed in studies showing that Raman measurements of carbonaceous matter can provide a reliable proxy for mineral-based determination of metamorphic grade (*e.g*., Nemanich and Solin, 1979). Thus, not only do the RIP values fit with variations in both the color and elemental (H/C and N/C) compositions of the kerogens here studied, but also the Raman spectra of the most altered kerogens mesh well with those representing early stages of a geochemically well-established sequence of alterations that in more metamorphosed terrains leads to the formation of graphite.

Refined by further studies—particularly, investigations of dehydrated particulate kerogens preserved by compression in, and isolated by acid maceration from, shales or siltstones (materials not investigated in the present work); and studies of kerogens from terrains having especially well-documented low-temperature histories, such as those investigated in the search for fossil fuels (Tissot and Welte, 1978; Durand, 1980; Hunt, 1996)—the RIP concept holds promise for development of a kerogen-based paleothermometer for use in submetamorphic and low-grade metamorphic geologic settings. Measurement of RIP values may thus prove useful in the petroleum industry by providing a quantitative and easily determinable indicator of the maturity of preserved organic matter in potential source rocks that is appreciably less subjective and more widely applicable than estimates based on the color and/or vitrinite reflectance of carbonaceous fossils or particulate sapropelic debris.

Biogenicity of ancient fossils

Over past decades, the rules for accepting Precambrian microfossil-like objects as *bona fide* have

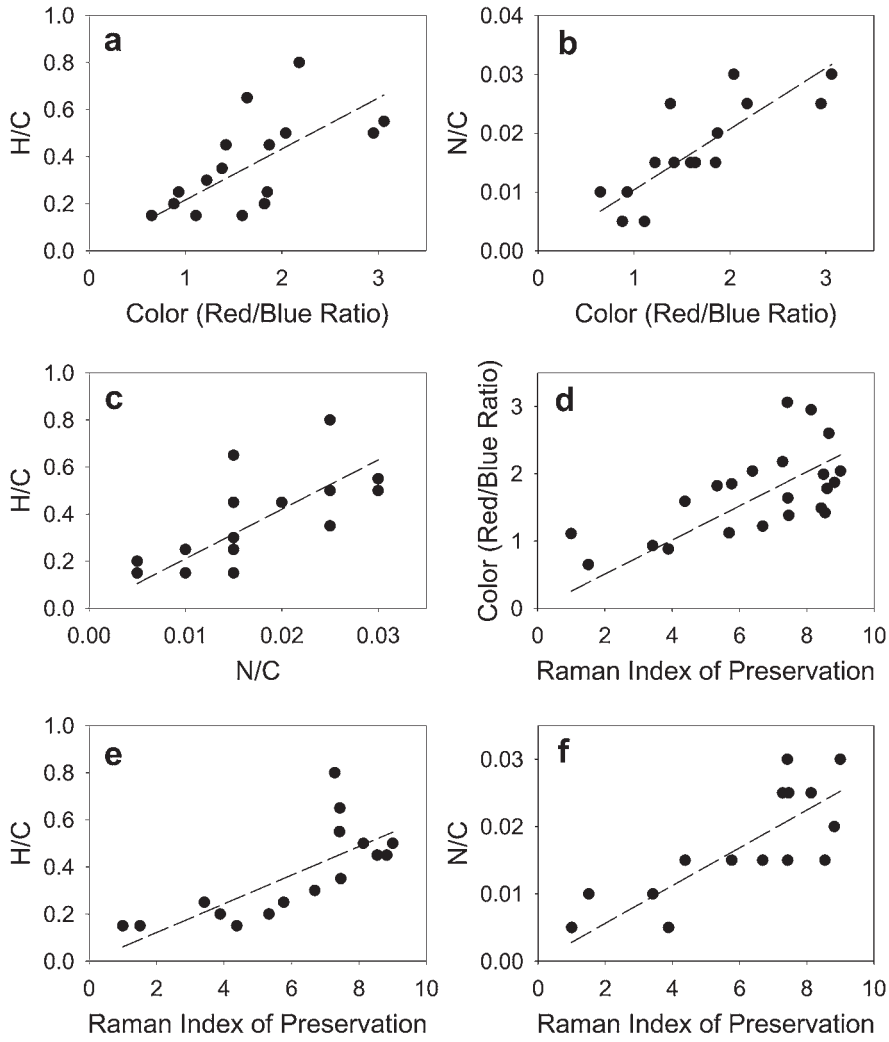

FIG. 12. Scatter diagrams and least-squares fit regression curves (denoted by dashed lines) showing correlations among various indicators of the geochemical maturity of kerogens permineralized in the fossil-bearing cherts studied here. The data plotted are those tabulated in Table 2. In each part, points denoting relatively more altered kerogens ("poorly preserved" fossils) are situated at the lower left, less altered kerogens ("well preserved" fossils) are situated toward the upper right. In the descriptions of each part, the "goodness of fit" of the data to the linear regression curve is expressed as r^2, the Coefficient of Determination. **a:** H/C ratios of bulk kerogens versus kerogen color measured in thin sections ($n = 16$; $r^2 = 0.37$). The more altered kerogens have low H/C ratios (<0.3) and are brownish-black in color (R/B ratios <1.0), whereas the less altered kerogens have higher H/C ratios (>0.5) and are brown or amber brown (R/B >1.5). **b:** N/C ratios of bulk kerogens versus kerogen color measured in thin sections ($n = 15$; $r^2 = 0.65$). The more altered kerogens have low N/C ratios (≤0.010) and are brownish-black in color (R/B ≤1.0), whereas the less altered kerogens have higher N/C ratios (≥0.025) and are brown or amber brown (R/B >1.5). **c:** H/C versus N/C of bulk kerogens ($n = 15$; $r^2 = 0.44$). The more altered kerogens have low ratios of both H/C (≤0.25) and N/C (≤0.010), whereas the less altered kerogens have higher ratios (H/C ≥0.4 and N/C ≥0.020). **d:** Kerogen color versus the RIP values of the preserved kerogens ($n = 22$; $r^2 = 0.28$). The more altered kerogens are brownish-black in color (R/B <1.0) and have low RIP values (<4.0), whereas the less altered kerogens are brown or amber brown (R/B >1.5) and have higher RIP values (>7.0). **e:** H/C ratios of bulk kerogens versus RIP values of the preserved kerogens ($n = 16$; $r^2 = 0.54$). The more altered kerogens have low H/C ratios (<0.3) and low RIP values (<7.0), whereas the less altered kerogens have higher H/C ratios (≥0.4) and higher RIP values (>7.0). **f:** N/C ratios of bulk kerogens versus RIP values of preserved kerogens ($n = 15$; $r^2 = 0.60$). The more altered kerogens have low N/C ratios (≤0.010) and low RIP values (<4.0), whereas the less altered kerogens have higher N/C ratios (≥0.015) and higher RIP values (>7.0).

come to be well established—namely, that such objects be demonstrably biogenic and be indigenous to and syngenetic with the formation of rocks of known provenance and well-defined Precambrian age (Schopf and Walter, 1983; Schopf, 2004). Of these criteria, the most difficult to satisfy has been that of biogenicity (Hofmann and Schopf, 1983; Schopf and Walter, 1983;

Mendelson and Schopf, 1992). As discussed below, Raman imagery seems particularly well suited to help solve this long-standing problem.

In a general sense, the answer to the question of biogenicity is straightforward, as was shown in the 1960s when early workers in the field first demonstrated that "Precambrian microfossils" are, indeed, true fossils (Barghoorn and Schopf, 1965; Barghoorn and Tyler, 1965; Cloud, 1965; Schopf, 1968). In answer to skeptics who conjectured about what sorts of nonfossils such objects seemingly "could be" or "might be" (Schopf, 1999a, p. 62), it was recognized early on that the critical problem was to establish what the "fossils" *actually* are. The solution was to establish their biological origin by showing that they possess a suite of traits that, taken together, are unique to life—a suite shared by such fossils and living microorganisms but not by inanimate matter (a formulation, it may be noted, essentially identical to that promulgated in the early 1800s by Baron Georges Cuvier, a founder of paleontology, as he sought to establish that megascopic fossils were not merely "sports of nature").

The early proposed multi-trait solution to the biogenicity problem, augmented today by lines of evidence unavailable years ago (such as measurements of the molecular–structural characteristics and isotopic compositions of the kerogen comprising individual microscopic fossils), is decidedly more powerful now than it was when it was first applied. Thus, though neither morphology (Hofmann and Schopf, 1983; Schopf and Walter, 1983; Mendelson and Schopf, 1992), nor carbonaceous makeup (Schopf and Walter, 1983; Schopf *et al*., 2002a,b; Pasteris and Wopenka, 2003), nor carbon isotopic composition (van Zuilen *et al*., 2002)—*if considered alone*—has proven consistently reliable as an indicator of biogenicity, the biologic origin of putative microscopic fossils can be established if such factors are considered together. For example, because (1) only living systems are known to be capable of producing biologic-like populations of cellular, morphologically diverse, microfossil-like objects composed of carbonaceous matter that exhibits a biological isotopic composition, (2) fossil-like objects that meet this suite of tests—such as the permineralized microorganisms of the Proterozoic Bitter Springs and Gunflint cherts (Barghoorn and Tyler, 1965; Schopf, 1968; Schopf and Blacic, 1971; House *et al*., 2000; Schopf *et al*., 2002a), two particularly well-studied examples of the 22 units investigated here—can be accepted as being assuredly biogenic.

Such traits, each typically composed of a nested series of factors and subfactors, constitute a cascade of evidence (*i.e*., if this is true, then this should be true, then this, and this, and this . . .) in which differing traits are used in differing situations, depending on the data available. Assuming that an appropriately biological set of traits is so used, this solution to the biogenicity problem could be shown to be in error only were it to be demonstrated that an identical suite of "biogenic" indicators is mimicked by assemblages of assuredly non-biologic microscopic objects—for instance, by showing for the Bitter Springs and Gunflint examples that biologic-like populations of diverse, cellular, carbonaceous, microfossil-like objects that exhibit a biological isotopic signature can be produced by solely abiotic processes.

Fossils analyzed from the 22 deposits studied here meet a series of 11 such tests. All exhibit (1) *biological morphology* (typically, a coccoidal or filamentous microbial organismal form), including (2) *structurally distinct carbonaceous cell walls* that define (3) *cell lumina* (originally cytoplasm-filled cell cavities). All occur in (4) *multi-member populations* (if one specimen can be preserved, others should be also) that include (5) *numerous taxa* (if one member of a biological community can be preserved, others should be also) and that exhibit (6) *taphonomically credible variable preservation* (ranging from life-like to degraded to markedly decomposed). All are (7) *preserved three-dimensionally by permineralization* (petrifaction) in fine-grained quartz, a common and well-understood mode of fossilization (Schopf, J.M., 1975) characteristic especially of organic-walled microorganisms (Mendelson and Schopf, 1992) and higher plants (*e.g*., petrified logs). Detailed morphometic data documenting (8) *biologically plausible size ranges* (Schopf, 1976, 1992b) have been published for 18 of the 22 assemblages (*viz*., for all but those of the Auburn Dolomite, River Wakefield Subgroup, and the Valukhtin and Yangzuang Formations, morphometrically unstudied assemblages for which diverse taxa have been illustrated; see Fig. 5 and references in Fig. 3). Fossils and co-occurring sapropelic debris in all but the most metamorphosed units studied exhibit (9) *the Raman signal of biogenic kerogen* (as defined herein and in Kudryavtsev *et al*., 2001), carbonaceous matter that in each of the 15 units thus far investigated (Strauss and Moore, 1992)—including

that comprising individual microscopic fossils (House *et al*., 2000)—has (10) *an isotopic composition typical of biologically produced organic matter*. Also, fossils in 16 of the units are (11) *preserved in stromatolites*, layered megascopic structures formed by mat-building microbial communities (Table 1).

Errors of interpretation made in recent astrobiological studies of fossil-like objects have stemmed largely from reliance on only one or two such biogenic indicators, rather than on a paleobiology-based suite of multiple traits such as that summarized above. For instance, McKay *et al*. (1996), on the basis chiefly of morphology, proposed that microscopic objects in the martian meteorite ALH84001 might be remnants of life. Even though they showed multiple examples of the microbe-like objects in question, their suggestion failed because the putative fossils lack cell lumina, carbonaceous cell walls, taphonomicaly credible variable preservation, and plausible biological size ranges (Bradley *et al*., 1997; Schopf, 1999b). Similarly, studies by García-Ruiz *et al*. (2002, 2003)—ingenious work that demonstrates the laboratory synthesis of organic-coated microbe-shaped mineralic objects, which they compared with Proterozoic and Archean petrified microfossils from numerous geologic units—miss the mark, not because the synthesized objects lack "biologic-like" morphology, but because unlike *bona fide* permineralized fossils they do not have cell lumina (being microscopic crystallites that lack the transverse septa that in true fossils define cellular cavities); their exteriors are organic-coated, rather than being bounded by structurally distinct carbonaceous walls (Kempe *et al*., 2002); the organic coatings (García-Ruiz *et al*., 2003) do not exhibit the Raman signature characteristic of kerogen (as defined by Kudryavtsev *et al*., 2001); and the objects are composed chiefly of witherite ($BaCO_3$), a mineral uncommon in the geologic record that is not known to play a role in fossil permineralization. As a final example, the recent report by Pasteris and Wopenka (2003) is similarly flawed. Despite these authors' claim that the nonbiologially produced carbonaceous objects they illustrate are "reminiscent of . . . some microfossils" (Pasteris and Wopenka, 2003, Fig. 3, p. 732), the opaque, evidently solid, carbonaceous particles they illustrate show no biologically distinctive morphologic traits (a deficiency not addressed, either by consideration of specific biologic characteristics or by comparison with particular modern or fossil analogues); the objects exhibit no evidence of cell lumina; they are not shown to have structurally distinct cell walls; and no data are presented to show that the objects have biologically plausible size ranges.

Use of Raman imagery can help avoid such errors. Not only does this technique provide means in putative microfossils to spatially correlate characteristic biological morphology with geochemically altered biological chemistry (Figs. 2–4), but it can be used also, by three-dimensional mapping (Schopf, 2003), to show the presence of cell lumina defined by degraded carbonaceous cell walls, a character in permineralized fossils central to establishment of biogenicity. Moreover, Raman analyses can provide telling data by which to discriminate between true fossils and more recently introduced contaminants (Tice *et al*., 2004) and—by use of the RIP concept—can provide a quantitative assessment of the geochemical maturity of the carbonaceous matter analyzed. Applied to the problem of biogenicity, analyses presented here of authentic fossils of diverse ages and variable low-temperature geological histories show that Raman imagery can provide molecular–structural data that link together a continuum of organically preserved specimens that ranges from well preserved to poorly preserved. Importantly, these analyses demonstrate that permineralized microorganisms composed even of partially graphitized kerogen can be morphologically identifiable (*e.g*., those of the River Wakefield Subgroup; Figs. 3e, 4e, 5, and cover of this issue of *Astrobiology*), and, thus, carbonaceous matter so altered that it no longer exhibits the distinctive Raman signal characteristic of relatively little altered kerogen (Kudryavtsev *et al*., 2001) can nevertheless be shown to be of biological origin.

CONCLUSIONS

Raman spectroscopy, a well-established technique for molecular–structural characterization of graphitized carbonaceous matter in metamorphosed geologic terrains (Pasteris and Wopenka, 1991, 2003; Jehlicka and Beny, 1992; Wopenka and Pasteris, 1993; Yui *et al*., 1996; Spotl *et al*., 1998; Jehlicka *et al*., 2003; Nestler *et al*., 2003), is applicable also to studies of the decidedly less altered (submetamorphosed and little metamorphosed) kerogens that comprise permineralized fossils and associated sapropelic debris. Such analyses are reported here of the carbonaceous matter perminer-

alized in 22 fossil-bearing cherts that range in age from Devonian (~400 Ma) to Paleoproterozoic (~2,100 Ma). Spectra acquired from rock-embedded fossils and sapropelic organic matter are for each such geologic unit essentially identical (Fig. 8), a reflection of their shared origin and geochemical history. These spectra, in turn, closely resemble those both of particulate kerogens isolated from such units by acid maceration and analyzed in aqueous media as well as those of well-preserved fossils experimentally heated to ≤600°C and analyzed *in situ*. Spectra of the relatively well-preserved specimens studied here exhibit an identifiable kerogen signal (Kudryavtsev *et al*., 2001) that evidences the presence of a complex mix of polycyclic, evidently interlinked, condensed aromatic hydrocarbons. In contrast, spectra of the more poorly preserved fossils—like those of rock-embedded fossils experimentally heated to >600°C—evidence varying stages of carbonization and graphitization. Finally, Raman spectra of dehydrated particulate kerogens extracted by acid maceration from the cherts here studied (including those of kerogens isolated from the least altered units) are composed of bands that are decidedly broader and more symmetrical than those of such materials measured *in situ*, spectral differences that mask the "kerogen signal" that are shown here to result from dehydration. That such changes in permineralized well-preserved kerogens are reversible with hydration suggests that new molecular–structural information may be retrievable from such dehydrated carbonaceous matter analyzed in earlier studies.

Raman imagery—an extension of Raman spectroscopy that by measuring large numbers of point spectra over a defined area, provides a means by which to correlate the chemical–structural characteristics of the materials analyzed with their optically discernible morphologies—is particularly suitable for analyses of ancient fossils. Used here to investigate the kerogenous components of fossil microscopic organisms and associated carbonaceous sapropel preserved in deposits subjected to low-grade (lower greenschist facies and below) metamorphism, such analyses of the low-temperature alteration of ancient organic matter are of potential use in petroleum exploration. Broadly applicable to problems of paleobiology, Raman imagery can be used to analyze ancient organic matter, whether in acid macerates or in thin sections, and to construct "molecular–structural maps" of permineralized fossils in both two and three dimensions. In addition, this technique provides data about the geochemical maturity and fidelity of preservation of the fossil organic matter analyzed in especially little altered fossils yielding information about original biochemical compositions (Czaja *et al*., 2002). Moreover, Raman imagery can help address questions about the biogenicity of ancient fossil-like objects, a long-standing problem in Precambrian paleobiology. Though Raman imagery links together only two of many traits that need to be considered in an evaluation of the origin of such putative fossils, the two factors it does address—cellular morphology and chemical–structural composition—are key to any biogenic interpretation. Shown here as being applicable to authentic microscopic fossils of diverse ages and geological histories, this technique, new to both paleobiologic and astrobiologic studies, holds great promise for future investigations of fossils, fossil-like objects, and associated organic materials, whether of Precambrian or extraterrestrial origin.

ACKNOWLEDGMENTS

For assistance, we thank E. Cholfin, L.A. Riedman, and J. Shen-Miller. For helpful reviews of this or an earlier version of this manuscript, we thank R.C. Burruss, J.M. Hayes, I.A. Kaplan, K.A. Kvenvolden, C. Marshall, M. Schoell, M.R. Walter, and an anonymous reviewer. This work was supported by NASA Exobiology Grants NAG5-12357 (to J.W.S.) and NAGW-4854/NAG5-4584 (to T.J.W.). Contributions to this study by A.B.K. were supported by the University of Alabama at Birmingham Center for Biophysical Sciences and Engineering and UCLA Sub-award 2090-G-DB152 (from the UCLA Institute of Geophysics and Planetary Physics Center for Astrobiology, Grant NCC2-1050). A.D.C. is an NSF Pre-Doctoral Fellow and a Fellow in CSEOL, the UCLA Institute of Geophysics & Planetary Physics Center for the Study of Evolution and the Origin of Life. The presence of the Raman imaging facility at the University of Alabama at Birmingham, where this work was carried out, is a consequence of the vision of Dr. Lawrence J. DeLucas.

ABREVIATIONS

PAH, polycyclic aromatic hydrocarbon; R/B, ratio of the red to the blue component; RGB, red,

green, and blue; RIP, Raman Index of Preservation; SD, standard deviation.

REFERENCES

Agrawal, U.P. and Ralph, S.A. (1997) FT-Raman spectroscopy of wood: Identifying contributions of lignin and carbohydrate polymers in the spectrum of black spruce (*Picea mariana*). *Appl. Spectrosc*. 51, 1648–1655.

Altermann, W. (2001) The oldest fossils of Africa—a brief reappraisal of reports from the Archean. *J. Afr. Earth Sci*. 33, 427–436.

Ambrose, G.J., Flint, R.B., and Webb, A.W. (1981) Precambrian and Palaeozoic geology of the Peake and Denison Ranges. *Geol. Surv. S. Aust. Bull*. 50, 1–71.

Arouri, K.R., Greenwood, P.F., and Walter, M.R. (2000) Biological affinities of Neoproterozoic acritarchs from Australia: Microscopic and chemical characterisation. *Org. Geochem*. 31, 75–89.

Awramik, S.M., Schopf, J.W., and Walter, M.R. (1983) Filamentous fossil bacteria from the Archean of Western Australia. *Precambrian Res*. 20, 357–374.

Awramik, S.M., Schopf, J.W., and Walter, M.R. (1988) Carbonaceous filaments from North Pole, Western Australia: Are they fossil bacteria in Archean stromatolites? A discussion. *Precambrian Res*. 39, 303–309.

Barghoorn, E.S. and Schopf, J.W. (1965) Microorganisms from the late Precambrian of central Australia. *Science* 150, 337–339.

Barghoorn, E.S. and Tyler, S.A. (1965) Microorganisms from the Gunflint chert. *Science* 147, 563–577.

Bekker, A., Holland, H.D., Wang, P.-L., Rumble, D. III, Stein, H.J., Hannah, J.L., Coetzee, L.L., and Beukes, N.J. (2004) Dating the rise of atmospheric oxygen. *Nature* 427, 117–120.

Beyssac, O., Goffe, B., Chopin, C., and Rouzaud, J.N. (2002) Raman spectra of carbonaceous material in metasediments: A new geothermometer. *J. Metamorphic Geol*. 20, 859–871.

Beyssac, O., Goffe, B., Petitet, J.-P., Froigneux, E., Moreau, M., and Rouzand, J.-N. (2003) On the characterization of disordered and heterogeneous carbonaceous materials by Raman spectroscopy. *Spectrochim. Acta* A59, 2267–2276.

Bickford, M.E., Soegaard, K., Nielsen, K.C., and McLelland, J.M. (2000) Geology and geochronology of Grenville-age rocks in the Van Horn and Franklin Mountains area, west Texas: Implications for the tectonic evolution of Laurentia during the Grenville. *GSA Bull*. 112, 1134–1148.

Bloeser, B., Schopf, J.W., Horodyski, R.J., and Breed, W.J. (1977) Chitinozoans from the Late Precambrian Chuar Group of the Grand Canyon, Arizona. *Science* 195, 676–679.

Boyce, C.K., Hazen, R.M., and Knoll, A.H. (2001) Nondestructive, *in situ*, cellular-scale mapping of elemental abundances including organic carbon of permineralized fossils. *Proc. Natl. Acad. Sci. USA* 98, 5970–5974.

Bradley, J.P., Harvey, R.P., and McSween, H.Y. Jr. (1997) No "nanofossils" in martian meteorite. *Nature* 390, 454–456.

Brasier, M.D., Green, O.R., Jephcoat, A.P., Kleppe, A.K., Van Kranendonk, M.J., Lindsay, J.F., Steele, A., and Grassineau, N.V. (2002) Questioning the evidence of Earth's oldest fossils. *Nature* 416, 76–81.

Brasier, M., Green, O., Jephcoat, A., Lindsay, J., and Steele, A. (2004) Earth's oldest (~3.5 Ga) fossils and the 'early Eden hypothesis': Questioning the evidence. *Origins Life Evol. Biosphere* 34, 257–269.

Bridgwater, D., Allaart, J.H., Schopf, J.W., Klein, C., Walter, M.R., Barghoorn, E.S., Strother, P., Knoll, A.H., and Gorman, B.E. (1981) Microfossil-like objects from the Archaean of Greenland: A cautionary note. *Nature* 289, 51–53.

Buick, R. (1984) Carbonaceous filaments from North Pole, Western Australia: Are they fossil bacteria in Archean stromatolites? *Precambrian Res*. 24, 157–172.

Buick, R. (1988) Carbonaceous filaments from North Pole, Western Australia: Are they fossil bacteria in Archean stromatolites? A reply. *Precambrian Res*. 39, 311–317.

Cady, S., Farmer, J.D., Grotzinger, J.P., Schopf, J.W., and Steele, A. (2003) Morphological biosignatures and the search for life on Mars. *Astrobiology* 3, 351–368.

Carlisle, D., Kettler, R.M., and Swanson, S.C. (1980) *National Uranium Resource Evaluation: Geological Study of Uranium Potential of the Kingston Peak Formation, Death Valley Region, California*, U.S. Department of Energy, Grand Junction, CO.

Castiglioni, C., Mapelli, C., Negri, F., and Zerbi, G. (2001a) Origin of the *D* line in the Raman spectrum of graphite: A study based on Raman frequencies and intensities of polycyclic aromatic hydrocarbon molecules. *J. Chem. Phys*. 114, 963–974.

Castiglioni, C., Negri, F., Rigolio, M., and Zerbi, G. (2001b) Raman activation in disordered graphites of the $A_{1'}$ symmetry forbidden $k \neq 0$ phonon: The origin of the *D* line. *J. Chem. Phys*. 115, 3769–3778.

Cloud, P. (1965) Significance of the Gunflint (Precambrian) microflora. *Science* 148, 27–45.

Cloud, P. and Licari, G.R. (1968) Microbiotas of the banded iron formations. *Proc. Natl. Acad. Sci. USA* 61, 779–786.

Crawford, A.R. and Compston, W. (1973) The age of the Cuddapah and Kurnool Systems, southern India. *J. Geol. Soc. Aust*. 19, 453–464.

Czaja, A.D., Schopf, J.W., Strorrie-Lombardi, M.C., Kudryavtsev A.B., and Bhartia, R. (2002) Laser-Raman spectroscopic analysis of biochemical changes caused by fossilization. In *Abstracts, Astrobiology Science Conference*, NASA Ames Research Center, Moffett Field, CA, p. 162.

Dehler, C.M., Elrick, M., Karlstrom, K.E., Smith, G.A., Crossey, L.J., and Timmons, J.M. (2001) Neoproterozoic Chuar Group (~800–742 Ma), Grand Canyon: A record of cyclic marine deposition during global cooling and supercontinent rifting. *Sediment. Geol*. 141-142, 465–499.

Diver, W.L. (1974) Precambrian microfossils of Carpentarian age from Bungle Bungle Dolomite of Western Australia. *Nature* 247, 361–363.

Durand, B., ed. (1980) *Kerogen, Insoluble Organic Matter from Sedimentary Rocks*, Éditions Technip, Paris.

Durand, B., Marchand, A., Amiell, J., and Combaz, A. (1977) Etude de kérogènes par résonance paramagnétique électronique. In *Advances in Organic Geochemistry 1975*, ENADIMSA, Madrid, pp. 753–779.

Ellery, A.D. and Wynn-Williams, D. (2003) Why Raman spectroscopy on Mars?—A case of the right tool for the right job. *Astrobiology* 3, 565–579.

Endo, M., Kim, C., Hiraoka, T., Karaki, T., Nishimura, K., Matthews, M.J., Brown, S.D.M., and Dresselhaus, M.S. (1998) Structural characterization of carbons from polyparaphenylenes prepared by the Kovacic and Yamamoto methods. *J. Mater. Res*. 13, 2023–2030.

Fairchild, T.R., Schopf, J.W., Shen-Miller, J., Guimarães, E.M., Edwards, M.D., Lagstein, A., Li, X., Pabst, M., and Soares de Melo-Filho, L. (1996) Recent discoveries of Proterozoic microfossils in south-central Brazil. *Precambrian Res*. 80, 125–152.

Faulon, J.L., Vandenbroucke, M., Drappier, J.M., Behar, F., and Romero, M. (1989) 3D chemical model for geological macromolecules. *Org. Geochem*. 16, 981–993.

Fischbach, D.B. (1971) The kinetics and mechanism of graphitization. In *Chemistry and Physics of Carbon, Vol. 7*, edited by P.L. Walker, Jr., Marcel Dekker, New York, pp. 1–107.

Fitzer, E., Mueller, K., and Schaefer, W. (1971) The chemistry of the pyrolytic conversion of organic compounds to carbon. In *Chemistry and Physics of Carbon*, *Vol. 7*, edited by P.L. Walker, Jr., Marcel Dekker, New York, pp. 237–385.

Forsman, J.P. (1963) Geochemistry of kerogen. In *Earth Series Monograph 16*: *Organic Geochemistry*, edited by I.A. Berger, Pergamon, Oxford, pp. 148–182.

García-Ruiz, J.M., Carnerup, A., Christy, A.G., Welham, N.J., and Hyde, S.T. (2002) Morphology: An ambiguous indicator of biogenicity. *Astrobiology* 2, 353–369.

García-Ruiz, J.M., Hyde, S.T., Carnerup, A.M., Christy, A.G., Van Kranendonk, M.J., and Welham, N.J. (2003) Self-assembled silica-carbonate structures and detection of ancient microfossils. *Science* 302, 1194–1197.

Gilson, T.R. and Hendra, P.J. (1970) *Laser Raman Spectroscopy*, Wiley-Interscience, New York.

Gogotsi, Y.G. and Nickel, K.G. (1998) Formation of filamentous carbon from paraformaldehyde under high temperatures and pressures. *Carbon* 36, 937–942.

Gutjahr, C.C.M. (1966) Carbonization measurements of pollen-grains and spores and their application. *Leidse Geol. Meded*. 38, 1–29.

Gutstadt, A.M. and Schopf, J.W. (1969) Possible algal microfossils from the Late Precambrian of California. *Nature* 233, 165–167.

Hayes, J.M. (2004) Isotopic order, biogeochemical processes, and earth history. *Geochim. Cosmochim. Acta* 68, 1691–1700.

Hayes, J.M., Kaplan, I.R., and Wedeking, K.W. (1983) Precambrian organic geochemistry, preservation of the record. In *Earth's Earliest Biosphere, Its Origin and Evolution*, edited by J.W. Schopf, Princeton University Press, Princeton, NJ, pp. 93–134.

Hofmann, H.J. (1976) Precambrian microflora, Belcher Islands, Canada: Significance and systematics. *J. Paleontol*. 50, 1040–1073.

Hofmann, H.J. and Grotzinger, J.P. (1988) Shelf-facies microbiotas from the Odjick and Rocknest Formations (Epworth Group; 1.89 Ga), northwestern Canada. *Can. J. Earth Sci*. 22, 1781–1792.

Hofmann, H.J. and Schopf, J.W. (1983) Early Proterozoic microfossils. In *Earth's Earliest Biosphere, Its Origin and Evolution*, edited by J.W. Schopf, Princeton University Press, Princeton, NJ, pp. 321–360.

Horodyski, R.J. and Donaldson, J.A. (1980) Microfossils from the Middle Proterozoic Dismal Lakes Group, Arctic Canada. *Precambrian Res*. 11, 125–159.

Horodyski, R.J. and Donaldson, J.A. (1983) Distribution and significance of microfossils in cherts of the Middle Proterozoic Dismal Lakes Group, District of Mackenzie, Northwest Territories, Canada. *J. Paleontol*. 57, 271–288.

House, C.H., Schopf, J.W., McKeegan, K.D., Coath, C.D., Harrison, T.M., and Stetter, K.O. (2000) Carbon isotopic composition of individual Precambrian microfossils. *Geology* 28, 707–710.

Hunt, J.M. (1996) *Petroleum Geochemistry and Geology*, 2nd ed., W.H. Freeman, New York.

Joy, J.W., Willis, A.J., and Lacey, W.S. (1956) A rapid cellulose peel technique in palaeobotany. *Ann. Bot. Nova Scotia* 20, 635–637.

Jehlicka, J. and Beny, C. (1992) Application of Raman microspectrometry in the study of structural changes in Precambrian kerogens during regional metamorphism. *Org. Geochem*. 18, 211–213.

Jehlicka, J., Urban, A., and Pokorny, J. (2003) Raman spectroscopy of carbon and solid bitumens in sedimentary and metamorphic rocks. *Spectrochim. Acta* A59, 2341–2352.

Kaufman, A.J. and Xiao, S. (2003) High CO_2 levels in the Proterozoic atmosphere estimated from analyses of individual microfossils. *Nature* 425, 279–282.

Kelemen, S.R. and Fung, H.L. (2001) Maturity trends in Raman spectra from kerogen and coal. *Energy Fuels* 15, 653–658.

Kempe, A., Schopf, J.W., Altermann, W., Kudryavtsev, A.B., and Heckl, W.M. (2002) Atomic force microscopy of Precambrian microscopic fossils. *Proc. Natl. Acad. Sci. USA* 99, 9117–9120.

Klein, C. and Hurlbut, C.S. Jr. (1985) *Manual of Mineralogy (After James D. Dana)*, 20th ed., Wiley, New York.

Knight, D.S. and White, W.B. (1989) Characterization of diamond films by Raman spectroscopy. *J. Mater. Res*. 4, 385–393.

Knoll, A.H. and Barghoorn, E.S. (1976) A Gunflint-type microbiota from the Duck Creek Dolomite, Western Australia. *Origins Life* 7, 417–423.

Knoll, A.H., Strother, P.K., and Rossi, S. (1988) Distribution and diagenesis of microfossils from the Lower Proterozoic Duck Creek Dolomite, Western Australia. *Precambrian Res*. 38, 257–279.

Kudryavtsev, A.B., Schopf, J.W., Agresti, D.G., and Wdowiak, T.J. (2001) *In situ* laser-Raman imagery of Precambrian microscopic fossils. *Proc. Natl. Acad. Sci. USA* 98, 823–826.

Landis, C.A. (1971) Graphitization of dispersed cabonaceous material in metamorphosed rocks. *Contrib. Mineral. Petrol*. 30, 34–45.

Lespade, P., Al-Jishi, R., and Dresselhaus, M.S. (1982) Model for Raman scattering from incompletely graphitized carbons. *Carbon* 20, 427–431.

Licari, G.R. (1978) Biogeology of the late Pre-Phanerozoic Beck Spring Dolomite of eastern California. *J. Paleontol*. 52, 767–792.

Licari, G.R., Cloud, P., and Smith, W.D. (1969) A new chroococcacean alga from the Proterozoic of Queensland. *Proc. Natl. Acad. Sci. USA* 62, 52–62.

Lin-Vien, D., Colthup, N.B., Fateley, W.G., and Grasselli, J.G. (1991) *The Handbook of Infrared and Raman Characteristic Frequencies of Organic Molecules*, Academic Press, New York.

Lumb, M.D. (1978) Organic luminescence. In *Luminescence Spectroscopy*, edited by M.D. Lumb, Academic Press, London, pp. 93–148.

Mapelli, C., Castiglioni, C., Meroni, E., and Zerbi, G. (1999a) Graphite and graphitic compounds: Vibrational spectra from oligomers to real materials. *J. Mol. Struct*. 480/481, 615–620.

Mapelli, C., Castiglioni, C., Zerbi, G., and Müllen, K. (1999b) Common force field for graphite and polycyclic aromatic hydrocarbons. *Phys. Rev. B* 60, 12710–12725.

Marshak, S. and Alkmim, F.F. (1989) Proterozoic contraction/extension tectonics of the southern São Francisco Region, Minas Gerais, Brazil. *Tectonics* 8, 555–571.

Marshak, S. and Engelder, T. (1985) Development of cleavage in limestones of a fold-thrust belt in eastern New York. *J. Struct. Geol*. 7, 345–359.

Marshall, C.P., Mar, G.L., Nicoll, R.S., and Wilson, M.A. (2001) Organic geochemistry of artificially matured conodonts. *Org. Geochem*. 32, 1055–1071.

Marucci, A., Pimenta, M.A., Brown, S.D.M., Mathews, M.J., Dresselhaus, M.S., and Endo, M. (1999) Study of overtones and combinational bands in the Raman spectra of polyparaphenylene-based carbons. *J. Mater. Res*. 14, 3447–3454.

Matthews, M.J., Dresselhaus, M.S., Endo, M., Sasabe, Y., Takahashi, T., and Takeuchi, K. (1996) Characterization of polyparaphenylene (PPP)-based carbons. *J. Mater. Res*. 11, 3099–3109.

Matthews, M.J., Pimenta, M.A., Dresselhaus, G., Dresselhaus, M.S., and Endo, M. (1999) Origin of dispersive effects of the Raman D band in carbon materials. *Phys. Rev. B* 59, R6585–R6588.

McKay, D.S., Gibson, E.K. Jr., Thomas-Keprta, K.L., Vali, H., Romanek, C.S., Clemett, S.J., Chiller, X.D.F., Maechling, C.R., and Zare, R.N. (1996) Search for past life on Mars: Possible relic biogenic activity in Martian meteorite ALH84001. *Science* 273, 924–930.

McMillan, P.F. and Hofmeister, A.M. (1988) Infrared and Raman spectroscopy. *Rev. Mineral*. 18, 99–159.

Mendelson, C.V. and Schopf, J.W. (1992) Proterozoic and selected Early Cambrian microfossils and microfossil-like objects. In *The Proterozoic Biosphere, A Multidisciplinary Study*, edited by J.W. Schopf and C. Klein, Cambridge University Press, New York, pp. 865–951.

Moore, T.B. and Schopf, J.W. (1992) Geographic and geologic data for PPRG rock samples. In *The Proterozoic Biosphere, A Multidisciplinary Study*, edited by J.W. Schopf and C. Klein, Cambridge University Press, New York, pp. 603–693.

Negri, F., Castiglioni, C., Tommasini, M., and Zerbi, G. (2002) A computational study of the Raman spectra of large polycyclic aromatic hydrocarbons: Toward molecularly defined subunits of graphite. *J. Phys. Chem. A* 106, 3306–3317.

Nemanich, R.J. and Solin, S.A. (1979) First- and second-order Raman scattering from finite-size crystals of graphite. *Phys. Rev. B* 20, 392–401.

Nestler, K., Dietrich, D., Witke, K., Röβler, R., and Marx, G. (2003) Thermogravimetric and Raman spectroscopic investigations on different coals in comparison to dispersed anthracite found in permineralized tree fern *Psaronius* sp. *J. Mol. Struct*. 661-662, 357–362.

Nutman, A.P., Allaart, J.H., Bridgwater, D., Dimroth, E., and Rosing, M. (1984) Stratigraphic and geochemical evidence for the depositional environment of the early Archean Isua Supracrustal Belt, southern West Greenland. *Precambrian Res*. 25, 365–396.

Nyberg, A.V. and Schopf, J.W. (1981) Microfossils in stromatolitic cherts from the Proterozoic Allamoore Formation of West Texas. *Precambrian Res*. 16, 129–141.

Nyberg, A.V. and Schopf, J.W. (1984) Microfossils in stromatolitic cherts from the Upper Proterozoic Min'yar Formation, southern Ural Mountains, USSR. *J. Paleontol*. 58, 738–772.

Oberlin, A., Boulmier, J.L., and Villey, M. (1980) Electron microscopic study of kerogen microtexture. Selected critera for determining the evolution path and evolution stage of kerogen. In *Kerogen, Insoluble Organic Matter from Sedimentary Rocks*, edited by B. Durand, Éditions Technip, Paris, pp. 191–241.

Pasteris, J.D. and Wopenka, B. (1991) Raman spectra of graphite as indicators of degree of metamorphism. *Can. Mineral*. 29, 1–9.

Pasteris, J.D. and Wopenka, B. (2003) Necessary, but not sufficient: Raman identification of disordered carbon as a signature of ancient life. *Astrobiology* 3, 727–738.

Peters, K.E., Ishiwatari, R., and Kaplan, I.R. (1977) Color of kerogen as index of organic maturity. *Am. Assoc. Petrol. Geol. Bull*. 61, 504–510.

Preiss, W.V. (1987) *Bulletin 53: The Adelaide Geosyncline*, Department of Mines and Energy, Geological Survey of South Australia, Adelaide.

Riding, R. and Sharma, W. (1998) Late Paleoproterozoic (~1800–1600 Ma) stromatolites, Cuddapah Basin, southern India: Cyanobacterial or other bacterial microfabrics? *Precambrian Res*. 92, 21–35.

Rigolio, M., Castiglioni, C., Zerbi, G., and Negri, F. (2001) Density functional theory prediction of the vibrational spectra of polycyclic aromatic hydrocarbons: Effect of

molecular symmetry and size on Raman intensities. *J. Mol. Struct*. 563/564, 79–87.

Roberts, S., Tricker, P.M., and Marshall, J.E.A. (1995) Raman spectroscopy of chitinozoans as a maturation indicator. *Org. Geochem*. 23, 223–228.

Schafer, H.E., Chance, R.R., Sibley, R.J., Knoll, K., and Schrock, R.R. (1991) Conjugation length dependence of Raman scattering in a series of linear polyenes: Implications for polyacetylene. *J. Chem. Phys*. 94, 4161–4170.

Schopf, J.M. (1975) Modes of fossil preservation. *Rev. Palaeobot. Palynol*. 20, 27–53.

Schopf, J.W. (1968) Microflora of the Bitter Springs Formation, Late Precambrian, central Australia. *J. Paleontol*. 42, 651–688.

Schopf, J.W. (1974) Palaeobiology of the Precambrian: The age of blue-green algae. In *Evolutionary Biology*, *Vol. 7*, edited by T. Dobzhansky, M.K. Hecht, and W.C. Steere, Plenum Press, New York, pp. 1–43.

Schopf, J.W. (1975) Precambrian paleobiology: Problems and perspectives. *Annu. Rev. Earth Planet. Sci*. 3, 213–249.

Schopf, J.W. (1976) Are the oldest "fossils", fossils? *Origins Life* 7, 19–36.

Schopf, J.W. (1977) Biostratigraphic usefulness of stromatolitic Precambrian microbiotas: A preliminary analysis. *Precambrian Res*. 5, 143–173.

Schopf, J.W. (1992a) Paleobiology of the Archean. In *The Proterozoic Biosphere, A Multidisciplinary Study*, edited by J.W. Schopf and C. Klein, Cambridge University Press, New York, pp. 25–39.

Schopf, J.W. (1992b) Proterozoic prokaryotes: Affinities, geologic distribution, and evolutionary trends. In *The Proterozoic Biosphere, A Multidisciplinary Study*, edited by J.W. Schopf and C. Klein, Cambridge University Press, New York, pp. 195–218.

Schopf, J.W. (1992c) Atlas of representative Proterozoic microfossils. In *The Proterozoic Biosphere, A Multidisciplinary Study*, edited by J.W. Schopf and C. Klein, Cambridge University Press, New York, pp. 1055–1117.

Schopf, J.W. (1993) Microfossils of the Early Archean Apex chert: New evidence of the antiquity of life. *Science* 260, 640–646.

Schopf, J.W., ed. (1999a) *Cradle of Life, The Discovery of Earth's Earliest Fossils*, Princeton University Press, Princeton, NJ.

Schopf, J.W. (1999b) Life on Mars: Tempest in a teapot? A first-hand account. *Proc. Am. Philos. Soc*. 143, 359–378.

Schopf, J.W. (2003) 3-D Raman imagery and atomic force microscopy of ancient microscopic fossils [abstract]. *Eos Trans. Am. Geophys. Union* 84(46) (Fall Meet. Suppl.), F340.

Schopf, J.W. (2004) Earth's earliest biosphere: Status of the hunt. In *Developments in Precambrian Geology 12: The Precambrian Earth: Tempos and Events*, edited by P.G. Eriksson, W. Altermann, D.R. Nelson, W.U. Mueller, and O. Cateneanu, Elsevier, Amsterdam, pp. 516–539.

Schopf, J.W. and Blacic, J.M. (1971) New microorganisms from the Bitter Springs Formation (Late Precambrian) of the north-central Amadeus Basin, Australia. *J. Paleontol*. 45, 925–961.

Schopf, J.W. and Fairchild, T.R. (1973) Late Precambrian microfossils: A new stromatolitic biota from Boorthanna, South Australia. *Nature* 242, 537–538.

Schopf, J.W. and Prasad, K.N. (1978) Microfossils in *Collenia*-like stromatolites from the Proterozoic Vempalle Formation of the Cuddapah Basin, India. *Precambrian Res*. 6, 347–366.

Schopf, J.W. and Sovietov, Y.K. (1976) Microfossils in *Conophyton* from the Soviet Union and their bearing on Precambrian biostratigraphy. *Science* 193, 143–146.

Schopf, J.W. and Walter, M.R. (1983) Archean microfossils: New evidence of ancient microbes. In *Earth's Earliest Biosphere, Its Origin and Evolution*, edited by J.W. Schopf, Princeton University Press, Princeton, NJ, pp. 214–239.

Schopf, J.W., Ford, T.D., and Breed, W.J. (1973) Microorganisms from the Late Precambrian of the Grand Canyon, Arizona. *Science* 179, 1319–1321.

Schopf, J.W., Dolnik, T.A., Krylov, I.N., Mendelson, C.V., Nazarov, B.B., Nyberg, A.G., Sovietov, Y.K., and Yakshin, M.S. (1977) Six new stromatolitic microbiotas from the Proterozoic of the Soviet Union. *Precambrian Res*. 4, 269–284.

Schopf, J.W., Zhu, W.Q., Zu, Z.L., and Hsu, J. (1984) Proterozoic stromatolitic microbiotas of the 1400–1500 Ma-old Gaoyuzhuang Formation near Jixian, northern China. *Precambrian Res*. 24, 335–349.

Schopf, J.W., Kudryavtsev, A.B., Agresti, D.G., Wdowiak, T.J., and Czaja, A.D. (2002a) Laser-Raman imagery of Earth's earliest fossils. *Nature* 416, 73–76.

Schopf, J.W., Kudryavtsev, A.B., Agresti, D.G., Wdowiak, T.J., and Czaja, A.D. (2002b) Images of Earth's earliest fossils?—Reply. *Nature* 420, 477.

Siskin, M. and Katritzky, A.R. (1991) Reactivity of organic compounds in hot water: Geochemical and technological implications. *Science* 254, 231–237.

Sobolev, V.S., Lepezin, G.G., and Dobretsov, N.L. (1982) *Metamorphic Complexes of Asia, Metamorphic Map of Asia (1:5,000,000)*, Pergamon, Oxford.

Spotl, C., Houseknecht, D.W., and Jaques, R.C. (1998) Kerogen maturation and incipient graphitization of hydrocarbon source rocks in the Arkoma Basin, Oklahoma and Arkansas: A combined petrographic and Raman study. *Org. Geochem*. 28, 535–542.

Staplin, F.L. (1969) Sedimentary organic matter, organic metamorphism, and oil and gas occurrence. *Bull. Can. Petrol. Geol*. 17, 47–66.

Starmach, K. (1963) Blue-green algae from the Tremadocian of the Holy Cross Mountains (Poland). *Acta Palaeontol. Polonica* 8, 451–462.

Strauss, H. and Moore, T.B. (1992) Abundances and isotopic compositions of carbon and sulfur species in whole rock and kerogen samples. In *The Proterozoic Biosphere, A Multidisciplinary Study*, edited by J.W. Schopf and C. Klein, Cambridge University Press, New York, pp. 709–798.

Strauss, H., Des Marais, D.J., Hayes, J.M., Lambert, I.B., and Summons, R.E. (1992a) Procedures of whole rock and kerogen analysis. In *The Proterozoic Biosphere, A Multidisciplinary Study*, edited by J.W. Schopf and C.

Klein, Cambridge University Press, New York, pp. 699–708.

Strauss, H., Des Marais, D.J., Hayes, J.M., and Summons, R.E. (1992b) Concentrations of organic carbon and maturities, and elemental compositions of kerogens. In *The Proterozoic Biosphere, A Multidisciplinary Study*, edited by J.W. Schopf and C. Klein, Cambridge University Press, New York, pp. 95–99.

Tice, M.M., Bostick, B.C., and Lowe, D.R. (2004) Thermal history of the 3.5–3.2 Ga Onverwacht and Fig Tree Groups, Barberton greenstone belt, South Africa, inferred by Raman microspectroscopy of carbonaceous material. *Geology* 32, 37–40.

Tissot, B.P. and Welte, D.H. (1978) *Petroleum Formation and Occurrence*, Springer, New York.

Tyler, S.A. and Barghoorn, E.S. (1963) Ambient pyrite grains in Precambrian cherts. *Am. J. Sci*. 261, 424–432.

Tu, A.T. (1982) *Raman Spectroscopy in Biology: Principles and Applications*, John Wiley & Sons, New York.

Tuinstra, F. and Koenig, J.L. (1970) Raman spectrum of graphite. *J. Chem. Phys*. 53, 1126–1130.

Ubbelohde, A.R. and Lewis, F.A. (1960) *Graphite and Its Crystal Compounds*, Oxford University Press, London.

Ueno, Y., Isozaki, Y., Yurimoto, H., and Maruyama, S. (2001) Carbon isotopic signatures of individual Archean microfossils(?) from Western Australia. *Int. Geol. Rev*. 40, 196–212.

Vandenbroucke, M. (2003) Kerogen: From types to models of chemical structure. *Oil Gas Sci. Technol. Rev. IFP* 58, 243–269.

Vandenbroucke, M. and Largeau, C. (2004) Kerogen formation, evolution and structure. *Org. Geochem*. (in press).

van Krevelen, D.W. (1993) *Coal: Typology—Chemistry—Physics—Constitution*, 3rd ed., Elsevier, Amsterdam.

van Zuilen, M.A., Lepland, A., and Arrhenius, G. (2002) Reassessing the evidence for the earliest traces of life. *Nature* 418, 627–630.

Vidano, R.P., Fischbach, D.B., Willis, L.J., and Loehr, T.M. (1981) Observation of Raman band shifting with excitation wavelength for carbons and graphites. *Solid State Commun*. 39, 341–345.

Walter, M.R., Goode, A.D.T., and Hall, W.D.M. (1976) Microfossils from a newly discovered Precambrian stromatolitic iron formation in Western Australia. *Nature* 261, 221–223.

Walter, M.R., Hofmann, H.J., and Schopf, J.W. (1983) Geographic and geologic data for processed rock samples. In *Earth's Earliest Biosphere, Its Origin and Evolution*, edited by J.W. Schopf, Princeton University Press, Princeton, NJ, pp. 385–413.

Walton, J. (1928) A method of preparing sections of fossil plants contained in coal balls or in other types of petrifaction. *Nature* 122, 571.

Wang, A., Haskin, L.A., Lane, A.L., Wdowiak, T.J., Squyres, S.W., Wilson, R.J., Hovland, L.E., Manatt, K.S., Raouf, N., and Smith, C.D. (2003) Development of the Mars microbeam Raman spectrometer (MMRS). *J. Geophys. Res*. 108(E1), 5-1–5-18.

Wang, H. and Qiao, X. (1987) Proterozoic geotectonic units of China and the nature of their boundaries [in Chinese with English abstract]. *Precambrian Geol*. 3, 1–14.

Wicander, E.R. and Schopf, J.W. (1974) Microorganisms from the Kalkberg Limestone (Lower Devonian) of New York state. *J. Paleontol*. 48, 74–77.

Williams, K.P.J., Nelson, J., and Dyer, S. (1997) *The Renishaw Raman Database of Gemological and Mineralogical Materials*, Renishaw Tranducers Systems Division, Gloucestershire, UK.

Wopenka, B. and Pasteris, J.D. (1993) Structural characterization of kerogens to granulite-facies graphite: Applicability of Raman microprobe spectroscopy. *Am. Mineral*. 78, 533–557.

Xing, Y. and Liu, H. (1973) *Micropalaeoflora from the Sinian Subera of W. Hupeh and Its Stratigraphic Significance*, Institute of Geology and Mineral Resources, Chinese Academy of Science, Beijing.

Yui, T.-F., Huang, E., and Xu, J. (1996) Raman spectrum of carbonaceous material: A possible metamorphic grade indicator for low-grade metamorphic rocks. *J. Metamorphic Geol*. 14, 115–124.

Zhang, Y. (1981) Proterozoic stromatolite microfloras of the Gaoyuzhuang Formation (Early Sinian: Riphean), Hebei, China. *J. Paleontol*. 55, 485–506.

Zhang, Y. (1985) Stromatolitic microbiota from the Middle Proterozoic Wumishan Formation (Jixian Group) of the Ming Tombs, Beijing, China. *Precambrian Res*. 30, 277–302.

Address reprint requests to:
J. William Schopf
Department of Earth & Space Sciences
University of California
Los Angeles, CA 90095-1567

E-mail: Schopf@ess.ucla.edu